
| | |
|---|---|
| Title | Towards the automated identification of Chrysomya blow flies from wing images |
| Authors | Macleod, N; Hall, MJR; Wardhana, AH |
| Description | This is the pre-peer reviewed version of the following article: Macleod, N. , Hall, M. J. and Wardhana, A. H. (2018), Towards the automated identification of Chrysomya blow flies from wing images. Med Vet Entomol. . doi:10.1111/mve.12302, which has been published in final form at https://doi.org/10.1111/mve.12302. This article may be used for non-commercial purposes in accordance with Wiley Terms and Conditions for Self-Archiving. |
| Date Submitted | 2018-05 |

# Automated identification of *Chrysomya* blowflies from wing images

Norman MacLeod[1], Martin J. R. Hall[2] and April H. Wardhana[3]

[1] Department of Earth Sciences, The Natural History Museum, London, UK, [2] Department of Life Sciences, The Natural History Museum, London, UK, and [3] Indonesian Research Centre for Veterinary Science, Bogor, Indonesia

**Corresponding author:** Norman MacLeod, Department of Earth Sciences, The Natural History Museum, Cromwell Road, London, SW7 5BD, UK N.MacLeod@nhm.ac.uk

**Abstract.** The Old World screwworm fly (OWSF), *Chrysomya bezziana* (Diptera: Calliphoridae), is an important agent of traumatic myiasis and, as such, a major human and animal health problem. In order to implement OWSF control operations it is important to be able to determine the geographical origin of these disease vectors to discriminate between invading and endemic populations. Gross morphological and molecular studies have demonstrated the existence of two distinct lineages of this species, one African and the other Asian. Wing morphometry can be of substantial assistance in identifying the geographical origin of introductions of this pest species by providing diagnostic markers that complement molecular diagnostics. However, the location of the landmarks used in traditional geometric morphometric analysis can be time consuming and is subject to error caused by operator subjectivity. Here we report results of an image-based approach to geometric morphometric analysis for delivering wing-based geographic classifications. Results indicate that this approach can produce discriminations that are practically indistinguishable from more traditional landmark-based results. In addition, we show that the direct analysis of digital wing images can be used to discriminate between three species of *Chrysomya* blow flies of veterinary and forensic importance and between *C. bezziana* genders.

**Key Words.** morphometrics, Old World screwworm fly, *Chrysomya*, biogeography, species identification, sexual dimorphism.

## Introduction

The Old World screwworm fly (OWSF), *Chrysomya bezziana* (Diptera: Calliphoridae), is an important agent of traumatic myiasis in humans, but more importantly in animals who cannot protect themselves from fly infestation as efficiently as humans. As a result, traumatic myiasis is a worldwide animal health problem and the cause of severe economic losses, especially in developing countries (Hall *et al*., 2016). In organizing efforts to control outbreaks of traumatic myiasis in both animal and/or human populations it is important to determine the origin of the disease vectors as control strategies, and their targets, will differ depending on whether the outbreak is being caused by infestations of this species from indigenous or exogenous populations. Molecular studies have demonstrated the existence of considerable mitochondrial DNA *cytochrome-b* gene diversity between African and Asian populations (Hall *et al*., 2001; Wardhana *et al*., 2012). While these differences suggest that DNA barcoding may be used to make correct identification of specimens from African and Asian populations, as a practical consideration, *Chrysomya* monitoring efforts would be facilitated greatly if reliable morphological markers capable of performing these same identifications could be found. Fortunately, it is often the case that, once genetic distinctions between populations have been established, the careful comparison of patterns of morphological variation between genotypic variants has resulted in the recognition of such morphological markers (e.g., Hendrichs *et al*., 2015 and references therein).

In terms of seeking morphological targets that might potentially be useful for this purpose, the placement and form of wing-support veins, as well as the configuration of landmark point locations defined by wing-vein intersections or vertices, have often been found to be highly informative indicators of family, genus and species-level identification across many insect orders (Comstock and Needham, 1898, Johnson and Triplehorn, 2000). In particular, the configuration of support-vein vertices has proven especially well-suited to geometric morphometric studies as these vertices are one of the comparatively rare instances in which specific landmark locations conform to the definitions of both biological and topological homology (Morgan, 1912; Bookstein, 1991; Rohlf, 1993; Chesters *et al*., 2012; Hall *et al*., 2014; Quezada-Euán *et al*., 2015). Unfortunately, the location of support-vein vertices across an insect wing rarely exhibit an even distribution across the entire wing surface owing to the coalescence of the major veins in the pteralia, the hierarchical branching and radiation of these veins across the wing, the uneven spacing of major vein branchings, the uneven distribution of cross veins, and the progressive reduction in the sizes of post-branching secondary, tertiary and quaternary veins which often make the forms of these

branches, and configuration of their vertices, indistinct under microscopic inspection as well as in photomicrographs (Fig. 1A). Moreover, the exclusive (e.g., Rohlf, 1993; Chesters *et al*., 2012; Hall *et al*., 2014), and/or near exclusive (e.g., Quezada-Euán *et al*., 2015) morphometric focus on the configuration of wing-vein vertices effectively discards all non-vertex information about the forms of the wing margin and the geometry of the wing veins themselves, thus providing a highly biased sample of the actual wing morphology. Last, but not least, the collection of large numbers of landmark points from insect wing images is a labour-intensive, time-consuming, and error-prone process, thus compromising the utility of geometric morphometric data collection and analysis procedures in making a practical contribution to population and species-identification process. These issues will be especially problematic and limiting for animal husbandry and medical workers located in rural regions far from the locations of laboratories containing even basic microscopic imaging and morphometric data-collection systems (MacLeod, 1990; Beccara *et al*., 1993; Beccara, 1996).

Recently, geometric morphometric-style procedures have become available for use directly on digital images of the specimens of interest. Use of such image-bases data circumvents the need — at least in the first instance — to laboriously collect, process and analyze landmark and/or semilandmark data while still providing access to all the data-analysis tools, summaries, and model-based interpretive aids that give geometric morphometrics its extraordinary power to test morphology-based biological hypotheses (MacLeod *et al*., 2014; MacLeod, 2015, in press a). While the results of such digital image-based investigations are often sufficient to resolve morphological issues by themselves, these results can also be used in an exploratory mode to guide the development of more traditional geometric morphometric, landmark and semilandmark-based sampling schemes so that they can more informatively, more objectively, and more adequately capture those aspects of a sample's morphology that either exhibit pronounced patterns of variation or whose variation is especially pertinent to the resolution of a particular biological question or issue. In addition, this approach opens the door to full automation of a wide variety of taxonomic-identification procedures across the fields of biology, ecology, archaeology, anthropology, astronomy, acoustics, linguistics — essentially to any field in which the primary data of interest can be represented as a collection of digital images (see MacLeod, 2007a; MacLeod *et al*., 2013 for examples).

Owing to the recency of its development, applications of this new image-based approach to morphometric analysis have been few to date. In particular, no head-to-head comparisons of the identification results that can be achieved by this traditional approach and a traditional landmark-

based geometric morphometric analysis, have been published. So that such a comparison can be made in the context of population-level identifications of a well-known and economically deleterious disease vector, we herein present experimental results that document the extent to which either a traditional, landmark-based, geometric morphometric analysis of wing support vertex configurations, or a direct analysis of whole-wing morphologies, can be used to distinguish between African and Asian populations of *C. bezziana.*

In addition to our primary consideration of *Chrysomya bezziana* biogeography, this genus includes two other species that are facultative agents of traumatic myiasis in Asia, *C. megacephala* and *C. rufifacies* (Sukontason *et al.*, 2005). Both field and laboratory experience has shown that it can sometimes be difficult to discriminate between adults of these species via visual inspection, especially between females of *C. bezziana* and *C. megacephala* which most identification keys separate on the basis of subtle differences in frons morphology (Irish *et al*., 2014). Therefore, in addition to its use to identify the geographic affinities of disease agents and pathogen vectors, a simple morphometric tool that could deliver swift and accurate identifications of these species would be of considerable value. Such a tool would also benefit forensic studies as *C. megacephala* and *C. rufifacies* can develop on animal carrion, and thus would have forensic value as and indicator of minimum post-mortem interval. Accordingly, as a secondary objective of our investigation, we evaluate the utility of the direct analysis of whole-wing morphology to support the automated, species-level identification of *C. bezziana*, *C. megacephala* and *C. rufifacies.* Finally, we apply and compare the results obtained by the *C. bezziana* dataset to the question of sexual dimorphism, since it is only gravid females of this species that are vectors of traumatic myiasis.

## Materials

The samples of African *C. bezziana* were taken from the pinned collections of the Natal Museum and the National Collection of Insects, Pretoria, both in South Africa, and from The Natural History Museum, London (Hall *et al*., 2014). Male and female *C. bezziana* specimens from the island of Sumba were taken from a colony at the Parasitology Department of the Indonesian Research Centre for Veterinary Science, Bogor, established from larvae collected from a case of traumatic myiasis on Sumba, Indonesia (Hall *et al*., 2014). Samples of *C. megacephala* and *C. rufifacies* were collected as adults on Bezzilure-baited sticky traps (Sulston *et al.*, 2014) located in Indrapuri District on the

island of Sumatra, Indonesia. The Sumba and Sumatra samples of all species were preserved in 80 percent ethanol and maintained at -20°C until analysis.

## Methods

Digital images of isolated and slide-mounted wings were obtained using standard entomological photomicrography (Fig. 1A; Hall *et al.*, 2014). The majority of wings imaged were right wings. If left wings were imaged they were transformed into pseudo-right wing images by mirroring them across the anterior-posterior (*y*) axis using standard image processing procedures. No effort was made to 'clean up' these images or select only well-preserved, complete and intact (non-torn or damaged) specimens.

For the traditional geometric morphometric analysis 21 landmarks were selected to quantify wing morphology (Fig. 1B). These landmarks were defined on the basis of articulations between wing basal sclerites and wing veins, bifurcations of wing veins, intersections between primary and transverse wing veins, intersections between primary wing veins and the wing periphery, and the peripheral indentation that marks the boundary between the alulae and anal wing regions along the anal margin. Since these structures are biological homologues across the species consider by this investigation the majority of these landmarks are of the "type 1" variety (Bookstein, 1991). Owing to their unquestioned biological identity type 1 landmarks are widely considered to be the most reliable sources of evidence for documenting morphological similarities and differences in an evolutionary context.

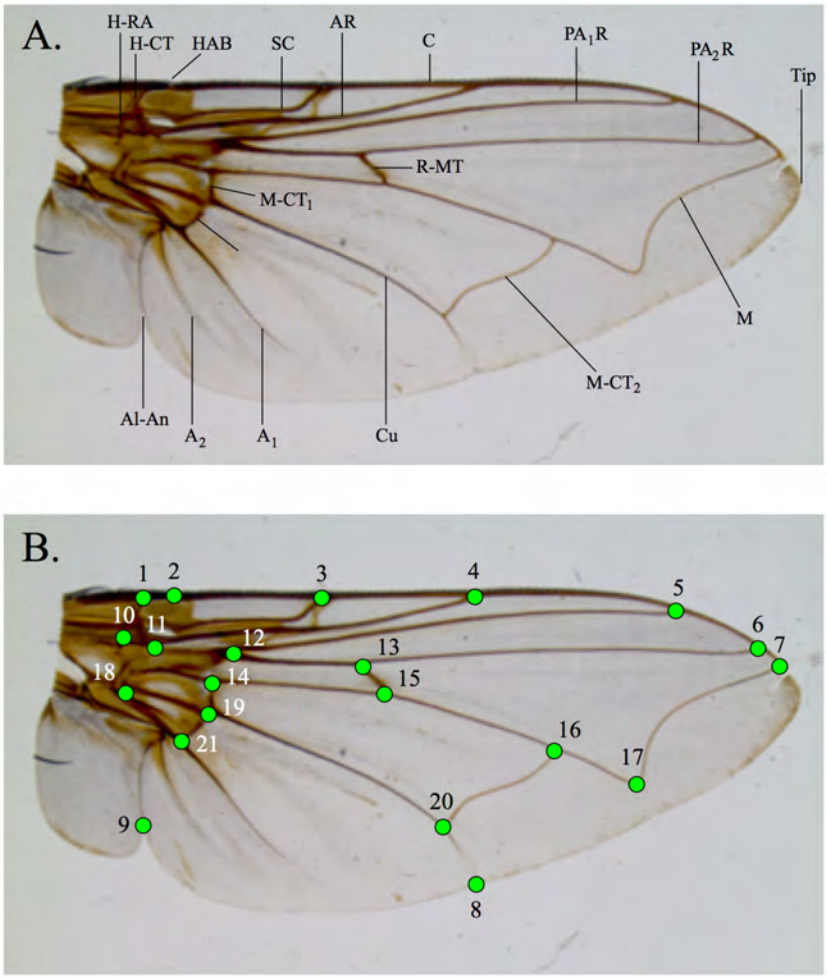


Figure 1. Morphology (A) and landmark-based sampling (B) of the *Chrysomya* wing. Morphological characters included the following humerus-radius articulation (H-RA), humerus-costa transverse vein (H-CT), costal margin (C), subcostal vein (SC), anterior radius vein (AR), first post-anterior radius vein (PA1R), second post-anterior radius vein (PA2R), wing tip (Tip), medial vein (M), radius-medial transverse vein (R-MT), cubital vein (Cu), proximal medial-cubital transverse vein (M-CT1), distal medial-cubital transverse vein (M-CT2), distal anal vein (A1), proximal anal vein (A2), cubital-distal anal transverse vein, alulal-anal indentation (Al-An). Landmarks: 1 - intersection between the humeral transverse vein and costal vein, 2 - position of the humeral articulation or break, 3 - intersection between the subcostal and costal veins, 4 - intersection between the anterior branch of the anterior radius vein (AR) and the costal margin (C), 5 - intersection between the first post-anterior branch of the radius vein (PA1R) and the costal margin (C), 6 - intersection between the second post-anterior branch of the radius vein (PA2R) and the costal margin (C), 7 - intersection between the medial vein (M) and the costal margin (C) or wing periphery, 8 - intersection between the cubital vein (Cu) and wing periphery, 9 - distal intersection between the anal and alulal areas (Al-Au), 10 - articulation between the humeral sclerite and the radius vein (H-RA), 11 - first bifurcation of the radius vein (AR) resulting the creation of this vein's anterior (AR) and first post-anterior (PA1R) branches, 12 - second bifurcation of the radius vein (AR) resulting the creation of this vein's first post-anterior (PA1R) and second post-anterior (PA2R) branches, 13 - anterior intersection between the radius-medial transverse vein (R-MT) and the second post-anterior radius vein (PA2R), 14 - anterior intersection between the distal medial-cubital transverse vein (M-CT1) and the medial vein (M), 15 - posterior intersection between the radius-media transverse (R-MT) vein and the medial vein (M), 16 - anterior intersection between the distal medial-cubital transverse vein (M-CT2) and medial vein (M), 17 - maxima of curvature in the distal portion of the medial vein (M), 18 - bifurcation between the cubital (Cu) and first anal (A1) veins, 19 - posterior intersection between the proximal medial-cubital transverse vein (M-CT1) and the cubital vein (Cu), 20 - posterior intersection between the proximal medial-cubital transverse vein (M-CT2) and cubital vein (CU), 21 - posterior intersection between the cubital-first anal transverse vein (C-AnT) and the first anal vein (A1). Specimen shown is BMNH E 1195306 which is a female African *C. bezziana*.

Despite the obvious utility of being able to match biologically corresponding point locations across a sample of forms, the level of biological specificity required to define these point locations accurately and completely also places severe constraints on the number and location of such landmarks on biological structures of interest. In this context, insect wings represent something of a 'best-case' scenario insofar as the density of sclerite articulations and vein bifurcations/intersections is such that a credible case can be made for the recognition of a comparatively large proportion of type 1 landmarks across these wings. However, even in this 'best-case' situation, the limitations of any attempt to represent complex biological structures via reference to a small number of carefully defined and corresponding landmark locations are apparent (see Introduction).

So long as the hypotheses under consideration are specifically and deterministically tied to landmark locations that can be sampled, this limitation does not present an insurmountable problem. Nevertheless, it is often the case that morphometric data analysts are asked to address hypotheses of a general and exploratory nature (e.g., Are two sets of forms or shape distinguishable morphologically from one another?). In such situations the limitations on the sampling of a form of interest via recourse to only a few relocateable mathematical points can result in the generality of the form's representation being compromised by the act of quantification. In effect, the constraints of traditional geometric morphometrics (see Bookstein, 1991; Costa and Cesar, 2000; Zelditch *et al*., 2004) can serve to enforce a confusion between the object under consideration — in this case the *Chrysomya* wing — and the manner in which these objects are being sampled for morphometric analysis.

Traditional geometric morphometrics forces the data analyst to select landmark locations *a priori,* for the most part without recourse to any information concerning which parts of the structure actually exhibit the greatest or least variation across the sample simply because it is those locations that *can* be represented by a landmark location, and then to accept the results of a morphometric analysis of that specific landmark configuration under the assumption that this configuration represents an adequate summary of geometric shape variation for the collection of forms or structures as a whole. This convention has become established as a result of geometric morphometrics conceptual derivation from multivariate morphometrics (under which identical sampling limitations apply, see Blackith and Reyment, 1971; Pimentel, 1979; Reyment *et al*., 1985, MacLeod in press) and as a result of the simple lack of any easily accessible alternative.

Such an alternative, however, now exists in the form of the direct analysis of digital image data that employs the same data-analysis conventions as geometric morphometrics (Turk and Pentland, 1991; MacLeod, 2014; 2015). Under this "eigenimage" approach the digital image frame is

regarded as constituting a Cartesian coordinate system analogous to that used to represent landmark configurations in traditional geometric morphometrics. But rather than representing forms in the sample by the Cartesian coordinates of point locations that are all regarded as being identical (= distinguishable from one another only by their differing locations with the Cartesian measurement system), the digital image-based analogue to geometric morphometrics regards the pixel grid (= the Cartesian coordinate system) as being a fixed set of topologically homologous locations whose individual coordinate locations need not be specified because they are all recorded for all images of interest. Rather, the form configuration of objects located within this system are specified by the brightness or color values of the individual pixels themselves. If these data are conceived as a topographic surface whose elevations above a base level are determined by the brightness of color values of the pixel elements, forms that are similar to one another will exhibit similarities in their pixel brightness/colour topologies while forms that differ will exhibit differences. Points of interest, such as the dark wing-vein vertices which, under a geometric morphometric sample scheme would be represented by different coordinate values would, in the image-based analogue to geometric morphometrics, be represented as brightness/color decreases at different pixel locations. But importantly, whereas traditional geometric morphometrics contains no information about the size, brightness, colour, etc. of the structures being represented by landmark coordinates, the image-based analogue to geometric morphometric quantification can easily be used to distinguish between such varying components of the form, or not, as the data-analysis situation demands.

The greater complexity — and so the information content — of pixel-based morphometric configurations can also be appreciated from the standpoint of that most basic of geometric morphometric form representations, the thin plate spline (Bookstein, 1989, 1991). In traditional geometric morphometrics thin plate splines are used to interpolate patterns of deformation across regions of the form not covered by landmarks based on the deformations observed at corresponding landmark locations. Thin plate splines can be used in an analogous way to represent interpolations of pixel colour/brightness values. But because these interpolations are tied to the pixel locations - locations that are arranged in an even grid across the entire form, the interpolation is able to take advantage of a much denser and more over sample spacing in the comparisons made between forms. Accordingly, the interpolation is more accurate and representative of the complete pattern of morphological variations that characterize forms. It is also possible to weight comparisons between forms in order to emphasize (or de-emphasize) the influence of particular features of the morphology by combining image-based, or eigenimage, morphometric analysis with various types of image processing procedures.

Under both traditional (landmark) and image-based approaches to morphometric analysis corrections for differences in the location, size and rotation of the forms in question can be made such that the conventions of Procrustes superposition are respected across datasets. In both cases the migration of particular features of the morphology can be tracked by their spatial displacements relative to the locations of surrounding features within other form or shape configurations. Most importantly, because the pixel-based representation of forms of interest includes all information present in the digital image there is no need to (1) define the location of particular features of interest *a priori*, (2) limit the analysis only to the tracking of those aspects of the form that can be defined by small sets of landmarks or by outline semilandmarks, and (3) limit the sample to include only those specimens that exhibit all *a priori*-selected features used to define the landmark and/or semilandmark locations. The relaxation of these strict comparability requirements that have become part and parcel of the traditional geometric morphometric approach to form and shape analysis renders this image and pixel-based approach a far more flexible — and so a more useful — tool for the exploration, discovery, documentation and interpretation of patterns of morphological variation within a sample. In addition, all the results-visualization and form/shape modeling tools that have been developed to facilitate geometric morphometric analysis can be applied in image-based morphometric investigations. Indeed, these tools are, if anything, more informative in the context of image-based morphometric analyses insofar as the entire set of features included in the image frame/matrix can be modeled and portrayed in a manner with which most researchers — and most audiences — are already familiar.

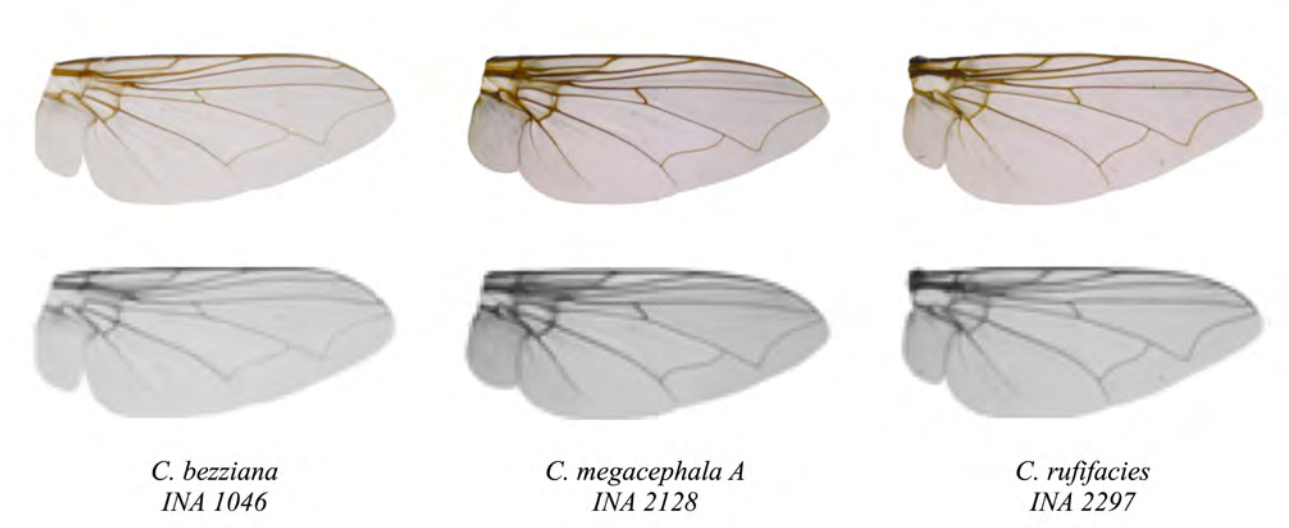


Figure 2. Original (upper row) and reduced resolution grayscale digital images of representative female specimens of the three species considered in this investigation.

In our *Chrysomya* investigation the same digital images that were used to quantify the positions of the 21 wing landmarks were trimmed to remove the background pixels while leaving a 10 percent pixel margin around the wing, down-sampled to ensure each frame conformed to a 40 x 100 pixel matrix, and converted from an 8-bit RBG to a 8-bit greyscale colorspace in order to minimize variation that might result from differences in specimen color (Fig. 2). Once in this format all wing images were aligned to such that their major axis was horizontal to, and centred within, the pixel frame. After alignment, each image was reformatted into a 4,000-term column vector of pixel brightness values, assembled into a data matrix, and submitted to a singular value decomposition (SVD)-based PCA in order to repack the observed image variation into the smallest number of statistically independent variables consistent with preservation of 95 percent of the original signal and projected as scores on these component axes. Following the placement of these image-based data in the PCA space their scores on all principal components comprising this 95 percent variation subset were submitted to a secondary canonical variates analysis (CVA, see MacLeod, 2007b) to create a space that maximized between-group separation relative to within-group dispersion (MacLeod, 2014; 2015a; 2015b). A bootstrap variant of the standard log-likelihood ratio test was used to estimate the statistical significance of the resultant group separations (Manly, 2006; MacLeod, 2015a; 2015b). Image models for both PCA and CVA axes were calculated using the method described by MacLeod (2009).

## Results

*Geography-Difference Test*

The dataset for this test consisted of 26 images of African *C. bezziana* female wings (20/26 right wings) and 20 images of Asian (Sumba) *C. bezziana* female wings (13/20 right wings). An initial PCA of the pooled landmark and image pixel brightness data showed that a comparatively small number of principal components were able to represent 95 percent of the shape variation recovered by the two alternative sampling schemes, 18 and 28 components respectively. Relative to the total number of specimens present in the original data matrices this operation resulted in a reduction of the effective dimensionality of these data of 60.9 and 39.1 percent.

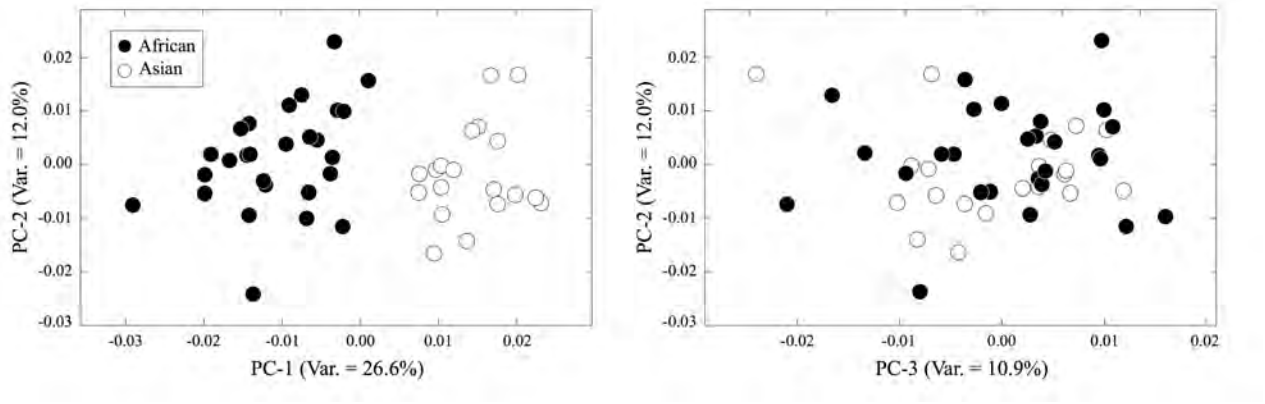


Figure 3. Projection of the *C. bezziana* Procrustes-aligned, wing landmark configurations into the space formed by the first three principal components of the shape covariance matrix. This subspace represents c. 50% of the shape variation recorded by these landmarks. Note strong separation between African and Asian populations within the PC-1 vs. PC-2 subspace and lack of obvious shape outliers.

*Landmark Results*.— A PCA of the landmark dataset identified the first three principal components as accounting for 26.6, 12.0 and 10.9 percent of the recorded shape variation respectively. All other principal components individually accounted for less than ten percent of the total shape variation. Scatterplots of this sample's landmark configurations projected into the space of these first three components shows clearly that the major source of variation in these data is accounted for by shape distinctions between the landmarked aspects of the wings of African and Asian populations (Fig. 3). Despite the small size of these samples no obvious shape outliers appear to be present in these plots, suggesting that these samples are fully representative of the populations from which they were derived.

A clear separation between geographic populations is evident along PC-1. A chord connecting the centroids of these populations in the PC-1 versus PC-2 subspace lies at an angle to the PC-1 axis, indicating that as aspect of wing-shape variation captured by this axis is also responsible for the observed shape variation. This orientation indicates that the optimal discriminant axis between these two populations incorporates aspects of shape variation represented by both PC-1 and PC-2, as well as (most likely) by other PC axes along which the distribution of these populations is more difficult to interpret qualitatively. In order to optimize this geographic discrimination and test the hypothesis of consistent and statistically significant group separation, the scores obtained from the projections of these landmark configurations on all 18 PC axes necessary to summarize 95 percent of the recovered shape variation were submitted to a CVA and the projections of these geographic group-specific configurations upon the single discriminant axis inspected for their distribution (Fig. 4).

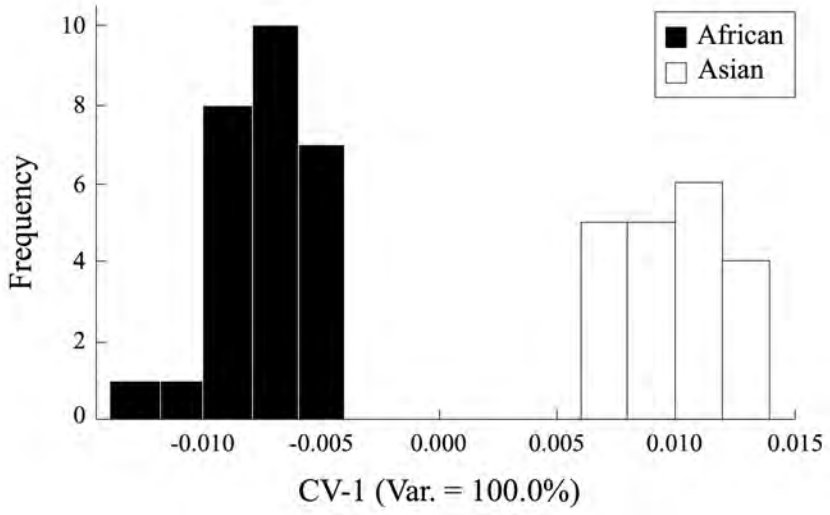


Figure 4. Frequency histogram of projected *C. bezziana* wing landmark configurations on the CVA discriminant axis separating African and Asian (Sumba) populations. This between-groups separation is significant at the $\alpha < 0.01$ level as assessed by a bootstrap test of the log-likelihood ratio index.

As was indicated by the PCA result, the configurations of these 21 wing landmarks contain sufficient information to allow African *C. bezziana* populations to be distinguished cleanly and consistently from Asian (Sumba) populations. The small number of specimens that were able to be included in this analysis might lead some to suspect the statistical significance and stability of this result. However, a bootstrapped test for the significance of the log likelihood ratio value ($\phi = 106.1$) was found to exceed all $\phi$-values calculated for 1,000 nonparametric, random pseudoreplicate datasets drawn from the original data (with replacement) by a considerable degree. Based on this result the statistical significance of the landmark configurations representing African and Asian population wing-shape difference is high, at least insofar as these populations are represented by this sample. With regard to the stability of this discriminant result, a jackknife (leave one out) analysis of the ability of this dataset to identify specimens of known geographic provenance as if they were unknown specimens (pseudo-unknowns) resulted in only a single misidentification of an African specimen for an Asian specimen. For the sample under consideration this translates into a robust estimated correctness ratio of 97.9 percent.

A precise morphological interpretation of this discriminant result can be formulated by back-projecting the coordinate locations of different steps along this between-group discriminant axis (see Fig. 4) into the PCA space and using the eigenvector equations that define this space to reconstruct landmark configurations that summarize shape difference between typical African and

typical Asian conditions. Figure 5 summarizes results of this modelling exercise for models calculated from all 18 of the PC variables that contributed to the CVA result.

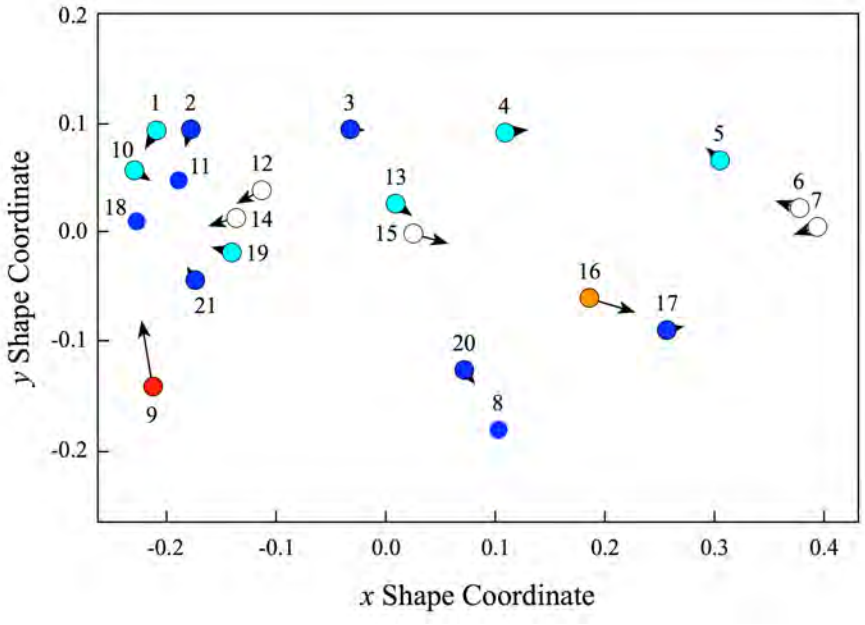


Figure 5. Directions of landmark migration between typical African (landmark configuration and displacement vector tails) and Asian (displacement vector heads) wings. See Fig. 1 for landmark names and defining criteria. The length of these vectors has been exaggerated (x3) in order to illustrate their directions and relative magnitudes. In addition, the landmark icons have been colour-coded to classify them into relative change categories: blue - no or small change, white - moderate change, yellow and orange - strong change, red - strongest change. See text for discussion.

Using these landmark displacement patterns as a guide to regional differences between typically African and typically Asian (Sumba) *C. bezziana* wings it would appear the former are characterized by a relatively larger basal region exhibiting greater distances between the humerus-radius articulation, intersection between the humerus-costal transverse vein, the humeral break and both the first proximal radius and cubital-anal vein bifurcations. Asian populations of this species exhibit a more compact placement of these features in the basal area typically. Along the costal wing margin Asian (Sumba) populations exhibit a modest outboard migration of the subcostal and first anterior radius vein termini accompanied by an inboard migration of the first and second post-anterior radius vein and medial vein termini. This contrast appears to grow more intense with distance along the wing margin. The strong inboard migration of the two outermost costal margin landmarks imparts an increase in the overall rounding of the wing tips in Asian (Sumba) populations relative to their African counterparts. This wing-tip rounding is also associated with an overall distal broadening of wing in Asian (Sumba) populations, which is reflected in these

landmark locations by the strong outboard and posterior migration of the medial-cubitus transverse vein, and the distal portion of the medial vein. Finally, the most striking single distinction between African and Asian (Sumba) *C. bezziana* wings is the very strong inboard migration of the marginal boundary between the alulal and anal regions of the wing in the vicinity of the jugal fold that appears characteristic of Asian (Sumba) populations.

*Image Results*.— A PCA of the image covariance matrix of the pooled African/Asian (Sumba) *C. bezziana* sample indicated that 28 latent variables were needed to represent 95 percent of the morphological variation recorded by these 40 x 100 pixel images. The first three of these components represent almost 60 percent of this variation with no subsequent component representing more than five percent of the total. Figure 6 illustrates the distribution of image pixel configurations projected into the subspace formed by these first three components.

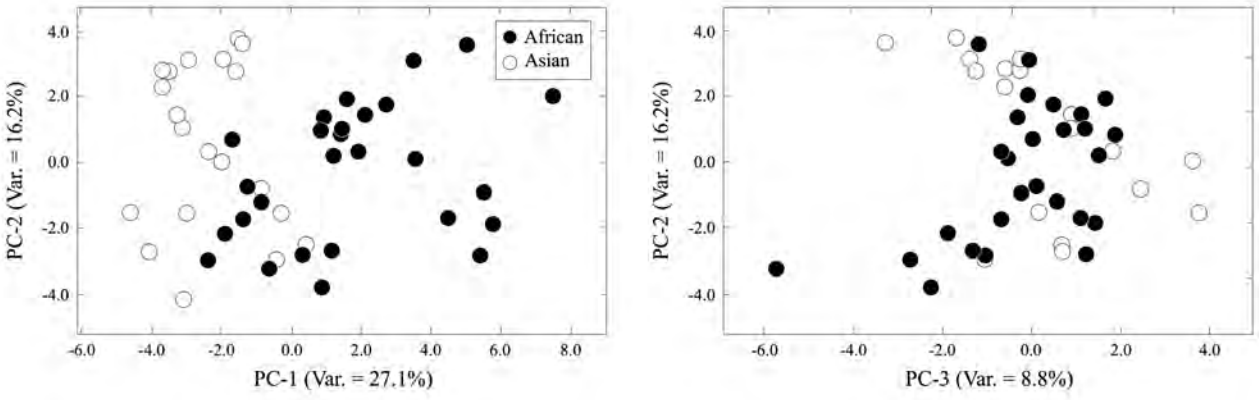


Figure 6. Projection of the African and Asian (Sumba) *C. bezziana* major axis-aligned, wing image configuration data into the subspace formed by the first three principal components of the image covariance matrix. This subspace represents c. 60% of the shape variation recorded by the reduced resolution wing images. Note strong, but not perfect, separation between African and Asian (Sumba) populations within the PC-1 vs. PC-2 subspace, presence of several morphological subclusters, and presence of obvious shape outliers

Direct comparison of these PCA results with those obtained from the landmark-based representation of these same images (Fig. 3) is instructive. First and most notably, although the major axis of wing image variation is obviously aligned with the distinction between African and Asian (Sumba) populations, the separation between these two groups for the image dataset is not mutually exclusive as it was in the landmark dataset. Rather, one — possibly two — distinct subgroups of African *C. bezziana* wings occupy the region of the Asian (Sumba) wing image space along the lower reaches of PC-1 and PC-2 as well as across the whole of PC-3. As is obvious from the PC-3 versus PC-2 subspace plot, this overlap between geographic populations is not as large as

it appears in the PC-1 versus PC-2 subspace. But overlap does exist. Moreover, the morphological diversity structure of these wings is far more evident in this image-based summary of shape variation than it was in the landmark-based summary. A very prominent discontinuity in image variation is evident in the image-based PC-1 vs PC-2 subspace as is the existence of several subsidiary subclusters of the African dataset as well as the existence of at least two distinct image outliers.

Figure 7 summarizes the patterns of wing image shape variation represented by the first three PC axes in the form of geometric models constructed at steps along each axis and summarized in the form of colorized image-difference maps. These synthetic images allow areas of weak (blue), intermediate (white) and strong (yellow-red) changes in pixel brightness values along each axis to be identified, tracked and interpreted in a manner that facilitates detailed geometric comparison/ interpretation of these models and, by extension, the image-based geometric spaces they represent. As was the case with the image-based PCA ordination space, it is instructive to compare these images with the analogous plot created for the landmark-based representation of these same images (Fig. 5) based on the CVA discriminant function which is dominantly aligned with the pooled-groups landmark data PC-1.

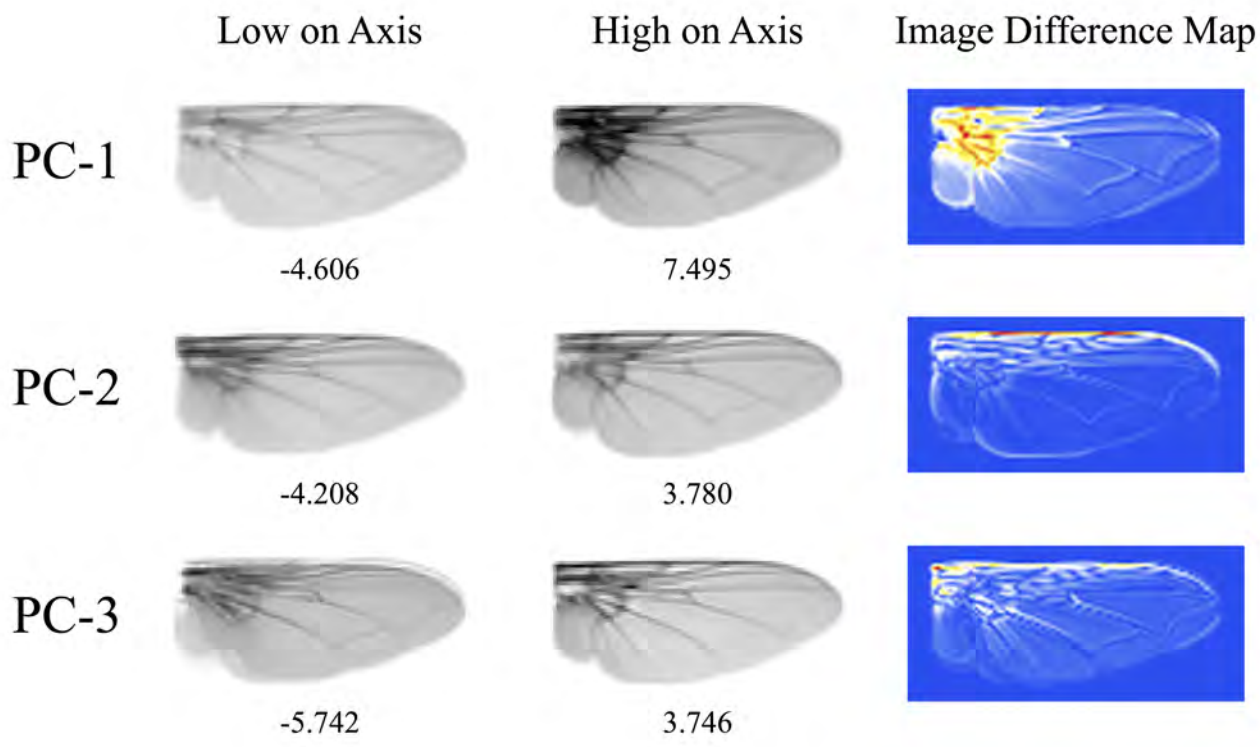

Figure 7. *Chrysomya bezziana* wing image models constructed at the ends of the of the distributions of image projections along each of the first three principal components of the image covariance matrix for the pooled (African-Asian [Sumba]) wing image data. Distinctions between these images represent the major modes of image variation on a pixel-by-pixel basis. Numbers below the hypothetical image models represent the coordinate values at which the models were constructed. The final column contains image difference maps in which the values of the differences between pixel brightness values have been colour-coded on the same continuous scale described in the Fig. 5 caption. See text for discussion.

Along PC-1 the primary mode of image-shape transformation involves the distinction between relatively light (low values) and relatively dark (high values) basal areas. Detailed comparison of modeled images at the ends of the PC-1 axis reveals that this darkening is associated with an inward migration for wing structural elements that involves a general shortening of the lengths of veins, vein articulations and the distances to vein bifurcations. It is noteworthy that this image-based PCA analysis was able to distinguish between a pronounced darkening of the inter-vein areas (coloured yellow on the PC-1 difference map in Fig. 7) and a stronger darkening that denotes a shift in the positions of the proximal portions of the costal margin, medial, cubital and first anal veins (coloured orange and red). As landmark datasets have no way to record any but spatial information this obvious darkening of the wing's basal area played no role in the landmark-based analysis. However, as can be seen in figures 6 and 7, all wings in our sample exhibiting dark basal areas dark basal areas are African with no Asian (Sumba) specimens exhibiting this wing characteristic (see supplementary data). Based on these results, a quick, easy, and relatively reliable test for Asian-African (Sumba) affinity might be implemented simply by looking for a dark, irregular splodge in the basal area of *C. bezziana* specimens.

Moderate levels of wing image shape change are also present in the traces of the subcostal, radius medial, cubital and anal veins with particularly pronounced variations occurring in the position of the radius-media transverse vein. On the whole these changes involve a migration of these features in anterior and basal directions to accommodate a general reduction in the width of the wing blade along a trend that becomes more pronounced along the wing's length. As a result, African *C. bezziana* wings exhibit more elliptical wings than Asian (Sumba) populations. In addition the anterio-posterior length of the alular area increases as PC-1 score increases or from typically Asian (Sumba) to typically African populations. The well-defined subcluster of African individuals (Fig. 6) lacks the darkened basal area and exhibits the less elliptical wing outline that characterizes the typically Asian (Sumba) morphology. The pronounced character of this morphological discontinuity is quite striking, both in the graphic summary provided by Figure 6 and in a visual overview of the entire African sample (see supplementary data).

Subsidiary modes of morphological variation in these wing images are expressed along the image-shape PC-2 and PC-3 axes. Along PC-2 this variation takes the form of an anterior migration of the costal margin relative to the traces of the subcostal and radius veins accompanied by a moderate posterior migration of the wing margin in the anal area along with a moderate left lateral migration of the alular margin. Both African and Asian (Sumba) populations exhibit wing morphologies that project to positions across the entire range of the PC-2 axis.

Similarly, patterns of morphological variation across PC-3 also dominantly involve the character of the costal margin, though in this case the primary focus of variation has shifted inboard to a position much more proximal to the wing's basal area. In addition, there appears to be a stabilization of variation involving the outline of the alular area from a multicharacter-state condition for wings that project to positions low on the PC-3 axis to a long and narrow form in wings that project to positions high on this axis. Although the present sample is too small to be certain, extreme African *C. bezziana* wings tend to project to positions low on this PC-3 axis while extreme Asian (Sumba) wings tend to project to positions high along this axis.

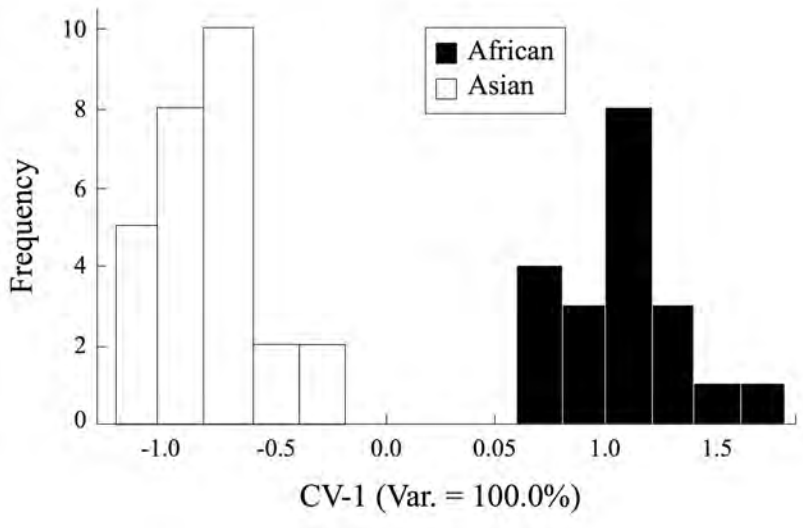


Figure 8. Frequency histogram of projected *C. bezziana* wing image configuration scores on PCs 1-28 onto the CVA discriminant axis separating African and Asian (Sumba) populations. The between-groups separation is significant at the $\alpha < 0.01$ level as assessed by a bootstrap test of the log-likelihood ratio index.

Despite the apparent overlap between African and Asian (Sumba) wing image configuration fields along PC-1 (see Fig. 6), when all 28 PC variables required to represent 95 percent of the recorded image configuration variation are included in a CVA analysis of these data African and Asian (Sumba) wing images are discriminated into mutually exclusive fields along the single linear

discriminant axis (Fig. 8). A non-parametric, bootstrapped, log-likelihood ratio test of group separation along this axis found that none of 1,000 pseudoreplicate datasets created randomly from these data (with replacement) produced $\phi$-index values greater than that calculated for this result ($\phi$ = 85.7). Accordingly, this result is interpreted as being statistically significant at greater than the $\alpha$ = 0.01 level.

While the raw confusion matrix for this result produced 100 percent correct results for the training set, a more rigorous jackknifed (leave one out) post-hoc identification test did detect a degree of instability in the CVA discriminant function with 7 of the 47 specimens being misidentified as a result of being treated as unknowns. This result translates into an overall stability-correctness estimate of 85.1 percent, which, while high, is substantially lower than the stability estimate achieved for the landmark data. Misidentifications were subequally divided among the two geographic populations with three African specimens being identified as Asian (Sumba) individuals and four Asian (Sumba) specimens being identified as African individuals.

Given the clear and unambiguous character of the between-groups separation achieved by the full CVA analysis, and in light of the observation that the African group, which was represented by the greater number of specimens ($n$ = 27 as opposed to $n$ = 20 for the Asian [Sumba] group), we feel confident that the stability of this discriminant result can be improved upon once a larger sample of both populations has been obtained. It might also be the case that increasing the spatial resolution of the images used in the analysis will also improve this result. But regardless of the fact that we do not advocate use of these geographic discriminant functions obtained for either the landmark or image configuration data until a larger sample of wing variation in these populations has been obtained, what these results do show, clearly, is that it is possible to reliably discriminate between geographic races of *C. bezziana* based on a morphometric characterization of wing shape alone. Moreover, given the time-consuming and somewhat specialist amount of labour involved in collecting landmark data from these wing images, it may be that, even if the wing image configuration results exhibit intrinsically more identification error than landmark-based results for the purpose of distinguishing between African and Asian *C. bezziana* populations by non-specialist agricultural workers in the field, a lower rate of identification accuracy would be tolerable, especially given the time, expense and contamination issues involved with implementation of both the landmark and molecular data-based alternatives. [Note: The presence of foreign material or damage can render landmark placement uncertain. Since landmark analysis are constrained by the need to be able to place all landmarks on all specimens both in the training set and on unknown specimens to be identified this source of error can have a large disruptive effect on “real world”

morphometric analyses. However, the greater information content of image data renders these sources of error less problematic for image-based morphometric analyses.]

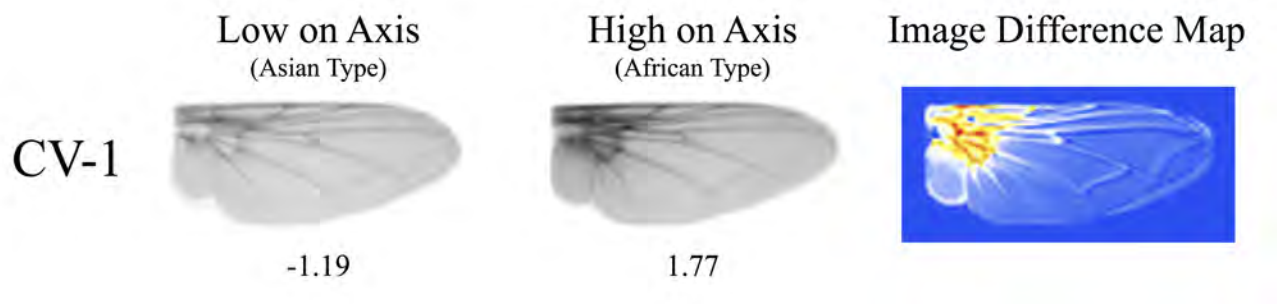


Figure 9. *Chrysomya bezziana* wing image models constructed at the ends of the of the distributions of image projections onto the linear discriminant axis (CV-1) that separates African and Asian (Sumba) wing image data. Distinctions between these images represent the major morphological distinctions between the wings of these populations on a pixel-by-pixel basis. Numbers below the hypothetical image models represent the coordinate values at which the models were constructed. The final graphic is an image difference map in which the values of the differences between pixel brightness values have been colour-coded on a continuous scale as described in the Fig. 5 caption. See text for discussion.

Figure 9 illustrates two hypothetical, end-member images calculated from the projected positions of typical African and Asian (Sumba) coordinate locations along the image CV-1 discriminant axis along with a pixel brightness difference map for the comparison of these two images. Close comparison with the PC-1 axis models included in Figure 7 shows that these models, along with the difference map, are almost identical with the pooled-groups PC-1 axis, an assessment that was confirmed by calculating the angle between these two vectors and computing a meta-difference map. Given the distribution of projected positions of African and Asian (Sumba) image configurations in the PC-1 versus PC-2 subspace (Fig. 6) this result is not surprising. Accordingly, the geometric interpretation detailed above for the pooled-groups PC-1 is essentially identical to that for the between-groups CV-1.

*Species-Difference Test*

As an additional test of the utility of morphometric procedures for extracting identifications from blowfly wing data that would be useful to medical and forensic researchers we summarize results of a species identification test. The dataset used for this test consisted of 20 wings from Asian (Sumba) female *C. bezziana*, 20 wings from Asian (Sumatra) female *C. rufifacies*, and 20 wings from Asian (Sumatra) female *C. megacephala*. The left-right composition of the former species was reported above. The *C. rufifacies* sample consisted of 16 right and 4 left wings. The *C. megacephala* sample

consisted only of right wings. As described in the Methods section, after tests for consistent differences between right and left wings of *C. rufifacies* returned negative results, the four left wings were transformed into pseudo-right wing images. Subsequent to this operation all images were processed according to the procedure described above (see Methods) This resulted in each wing being represented by a 100 x 40 pixel, major axis-aligned, grayscale image with the wing image centred on a white background (see supplementary files). The pixel matrices that constituted these images were then reformatted to constitute a 60 x 4000 data matrix and submitted to a SVD-based PCA for preliminary analysis.

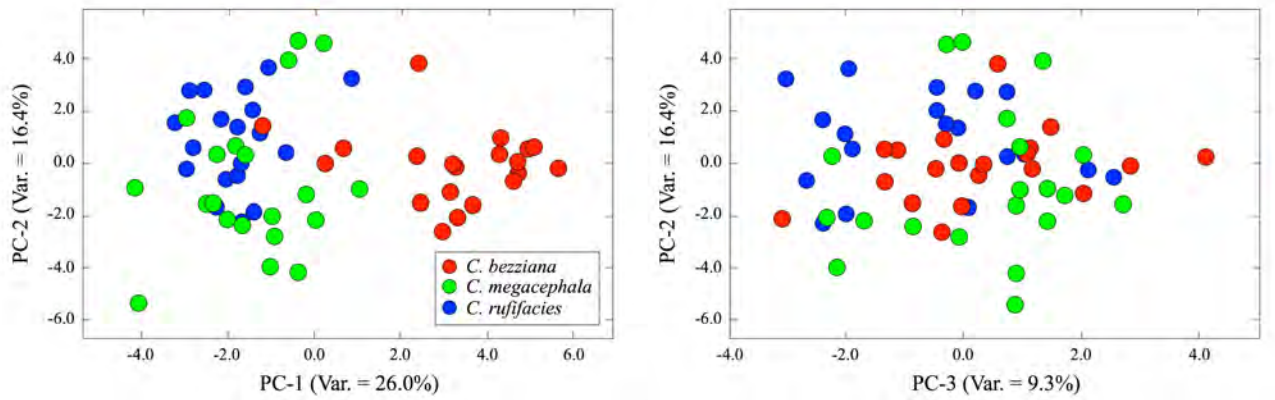


Figure 10. Projection of the *C. bezziana*, *C. megacephala*, and *C. rufifacies*, Procrustes-aligned, wing image configuration data into the space formed by the first three principal components of the image covariance matrix. This subspace represents c. 60% of the image variation recorded by the reduced resolution wing image dataset. Note the pronounced, but far from perfect, tendency toward species separation, relative distinctiveness of *C. bezziana*, and presence of wing configuration subgroups and outliers within both *C. bezziana* and *C. megacephala* within the PC-1 vs. PC-2 subspace.

Figure 10 illustrates the major dimensions of variation in the pooled species dataset. Together these three axes account for 58.35 percent of the pooled image configuration variation with only a single subsequent axis accounting for more than five percent of the remainder. For this PCA analysis 32 eigenvectors were necessary to represent 95 percent of the recorded image configuration variation. This represents a reduction in effective dimensionality of 46.7 percent in terms of the maximum number of components with positive eigenvalues and over a 99 percent reduction in dimensionality in terms of the number of variables that characterize the original images.

Based on these ordinations it is clear that typical *C. bezziana* wings differ in terms of their pixel configurations from *C. megacephala* and *C. rufifacies* and that this difference accounts for the major source of variation within the pooled dataset. What is less clear, however, is whether *C. megacephala* A and *C. rufifacies* can be distinguished from each other reliably from wing image

data alone. In terms of intrinsic variation within this dataset it is also clear that *C. bezziana* exhibits the greatest variance in wing pixel configuration and *C. rufifacies* the least.

Contrary to the previous two species-specific PCA results, the eigenvector orientations produced by this inter-specific analysis do not appear to be controlled by intra-specific variation in wing morphology. To be sure, one prominent pattern of intra-specific differentiation exists — the small subgroup of three *C. megacephala* specimens that exhibit anomalously high scores (for this species) along PC-2. However, since the PCA analysis is conducted on the pooled dataset, this intra-specific distinction does not exert a primary control on the placement of PC-2 as specimens as similar projected scores on this axis exist within the *C. bezziana* and *C. rufifacies* datasets.

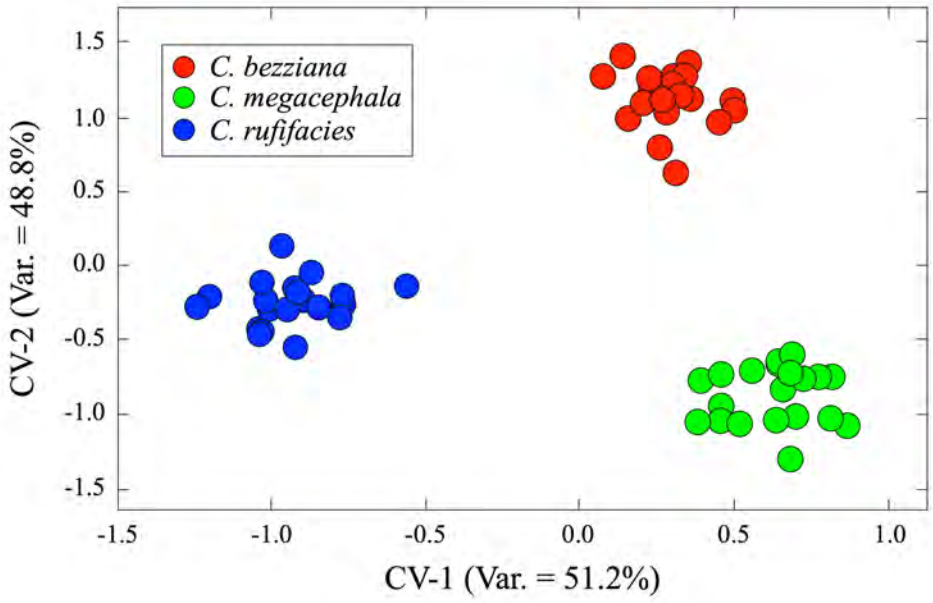


Figure 11. Projection of the *C. bezziana*, *C. megacephala A*, and *C. rufifacies*, scores on PCs 1-32 into the space formed by the two CVA discriminant axes. These axes represent 100% of the difference between group centroids in the linear, eigenvalue-standardized ordination space. Note tightness of variation within each of the species clusters, the clear and clean separation of species clusters from one another and the orientation of between-species distinctions relative to those of the discriminant axis vectors.

Notwithstanding the fact that the PCA analysis did not result in the complete separation of these three species along any the first three eigenvectors of the pooled image covariance matrix, when the information on wing morphological variation encoded by all 32 PCA scores necessary to represent 95 percent of the image-covariance structure are submitted to a CVA, the between-species differentiation that resulted was both clear and compelling (Fig. 11). Interestingly, the distinction between *C. bezziana* wing images and those of the other two species is not the most prominent differentiation pattern recorded by these data. Rather, *C. rufifacies* was identified as exhibiting the

most distinctive wing morphology, though only by a marginal amount. A more conservative — and perhaps more reasonable — interpretation of this discriminant result is that all three species' wing morphologies exhibit sub-equal patterns of uniqueness.

A non-parametric bootstrapped log-likelihood ratio test of group separation along this axis found that none of the 1000 pseudoreplicate datasets created randomly from these data (with replacement) produced $\phi$-index values greater than 120.0 whereas the $\phi$-index value calculated for this species-difference test was 261.1. Accordingly, this result is interpreted as being statistically significant at a level much greater than $\alpha = 0.01$. Moreover, irrespective of the small sample sizes involved in this test the discriminant result obtained for these data exhibited remarkably good stability (Table 1).

Table 1. Jackknifed confusion matrix for species-difference test CVA result.

| Species | *C. bezziana* | *C. megacephala* A | *C. rufifacies* | Total Correct | Group Total | Percent Correct |
|---|---|---|---|---|---|---|
| *C. bezziana* | 16 | 2 | 2 | 16 | 20 | 80.0 |
| *C. megacephala* A | - | 20 | - | 20 | 20 | 100.0 |
| *C. rufifaces* | 1 | - | 19 | 19 | 20 | 95.0 |
| Total Correct | 16 | 20 | 19 | 55 | 60 | 91.7 |
| Group Total | 17 | 22 | 21 | 60 | | |
| Percent Correct | 94.1 | 90.9 | 90.5 | 91.7 | | |

It is worth noting that the higher level of ambiguity seen in the jackknifed *C. bezziana* identifications is consistent with the PCA ordination having identified this species as exhibiting the most variable wing morphology of the three analysed here. This apparent intrinsic variability may may have implications for the performance of the PCA-CVA approach employed in this study with regard to the characterization of geographic populations (see above). Certainly it further strengthens the case for larger sample sizes to be used in order to obtain a more accurate and statistically robust model of morphological variation in the wings of these species. However, this result also throws the inherent ambiguity of the PCA result obtained for our data — and indeed all PCA results — into sharp focus in terms of their ability to deliver true representations of between-species distinctions. Through the years many morphometricians have come to rely on PCA ordinations to provide reliable estimates of group distinctiveness despite the fact that standard PCA analyses only operate on the pooled covariance or correlation matrices. The difference we have obtained between the group-level distinctions in the subspace formed by the first few PCA eigenvectors, compared to

those obtained from the same PCA data when subjected to a secondary CVA analysis, is striking and should be taken as a cautionary tale for those who rely on PCA-based ordination analyses for all morphometric analyses. The excellent stability characteristics of the CVA result obtained from these data also indicate that, even in cases when sample sizes are much smaller than the dimensionality of the original data, procedures are available that will allow data analysts to test specific hypotheses and obtain statistically valid results.

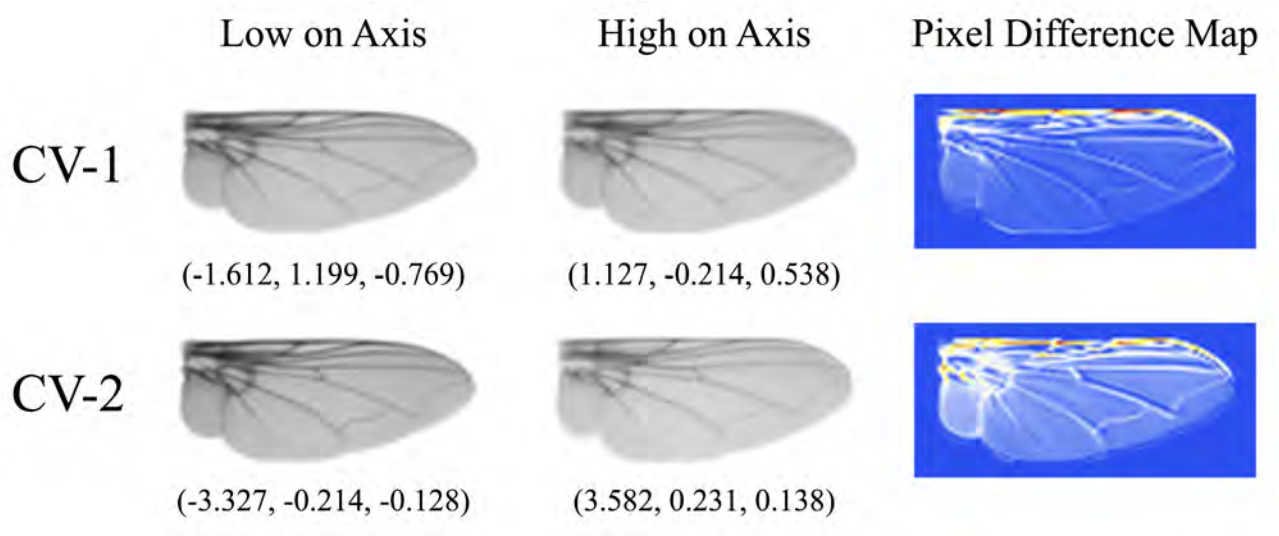


Figure 12. Wing image models constructed at the ends of the of the distributions of image projections along the two species-difference linear discriminant axes (CV-1, CV-2). Distinctions between these images represent the major models of digital image distinction on a pixel-by-pixel basis. Numbers below the hypothetical image models represent the coordinate values at which the models were constructed. The final column contains pixel difference maps in which the values of the differences between pixel brightness values have been colour-coded on a continuous scale as described in the Fig. 5 caption. See text for discussion.

Going beyond the question of whether wing morphology can be used to identify *Chrysomya* species, the results of our CVA-based analysis of *Chrysomya* wing images can also be used to guide the morphological interpretation of which wing characteristics differ between these three species. With regard to the difference between *C. rufifacies* and *C. bezziana/megacephala* expressed along CV-1, the former species is characterized by wings with thinner, more elliptical primary blades than those of the latter two species. This narrowing of the blade is associated with distal migration of the intersections between the costal margin and the subcostal, anterior radius and both first and second post-anterior radius veins, proximo-lateral migration of the medial cubital, and anal veins, and anterior migration of the anal blade margin. As a result of these modifications, *C. rufifacies* wings exhibit the most elliptically eccentric or pointed tips of the three species assessed in our study.

With regard to the interpretation of CV-2 which primarily captures the distinction between *C. megacephala* and *C. bezziana*, wings that project to positions low along this axis (= *C. megacephala*) are characterized by relatively narrow subcostal and anterior radial regions with more proximally placed intersections between (1) the costal margin, (2) the subcostal, anterior radius, and (3) both first and second post-anterior radius veins, with a more anteriorly placed second post-anterior, medial and cubital veins, and with a moderate posterior migration of the posterior wing margin in the mid-region of the blade. Conversely, wings that project to positions high along this axis (= *C. bezziana*) are characterized by slightly expanded subcostal and anterior radial regions with more distally placed intersections between the (1) costal margin, (2) the subcostal, anterior radius, and (3) both first and second post-anterior radius veins, with more posteriorly placed second post-anterior, medial and cubital veins, and with a pronounced posterior migration of the posterior wing margin in the distal region of the blade. Overall, these modifications impart a distinctly elliptical character to *C. rufifacies* wing, a moderately elliptical character to the *C. megacephala* wing, and a distinctly quadrate character to the *C. bezziana* wing.

*Gender-Difference Test*

The gender-difference dataset consisted of 20 images of Asian (Sumba) *C. bezziana* female wings and 24 images of Asian (Sumba) *C. bezziana* male wings. The female dataset consisted of 13 images of right wings and 7 images of left wings. The male dataset included 21 images of right wings and 3 images of left wings. After a preliminary investigation failed to find any consistent shape differences between right and left wings for either dataset, all left wing images were transformed into pseudo-right wing images and then processed according to the procedure described in the Methods section. At the end of this procedure each wing was represented by a 100 x 40 pixel, mean-aligned, grayscale image with the wing centred on a white background (see supplementary files). The pixel matrices that constituted these images were then reformatted to constitute a 44 x 4,000 data matrix and submitted to a PCA for preliminary analysis.

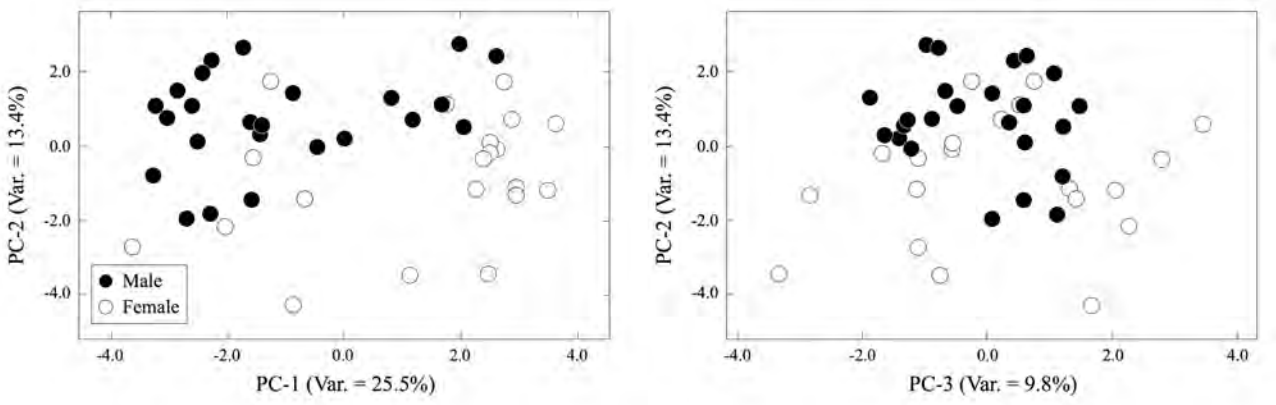


Figure 13. Projection of the *C. bezziana* major axis-aligned, wing image configuration data into the space formed by the first three principal components of the image covariance matrix for the gender-difference dataset. This subspace represents c. 48% of the image variation recorded by the reduced resolution image set. Note the strong, but not perfect, separation between male and female cohorts along PC-2, the presence of image configuration subgroups within the female dataset, and the difference in the image configuration variance between the two sexes.

Figure 13 illustrates the major dimensions of variation in the pooled gender-difference dataset. Together these axes account for 48.65 percent of the pooled image configuration variation with no subsequent axis accounting for more than eight percent of the remainder. For the PCA analysis a total of 27 component axes were necessary to represent 95 percent of the image configuration variation. This represents a reduction in effective dimensionality of 38.6 percent in terms of the maximum number of components with positive eigenvalues and a greater than 99.0 percent reduction in dimensionality in terms of the number of variables that were needed to characterize the original images. Based on these ordinations it is clear that typical male and female *C. bezziana* wings differ in terms of their pixel configurations and that this difference accounts for a major source of variation within the pooled dataset.

While both PCA ordination plots (Fig. 13) indicate that a broad difference between the sexes exists in terms of wing-shape variability, separation between species is largely the result of distinctions captured by PC-2 with a sub-dominant — but no less important — wing shape-difference component being supplied by PC-1. The shape variances along both PC-2 and PC-3 are much larger for the female dataset relative to the male dataset. Close inspection of the PC-1 versus PC-2 subspace suggests that this increase in shape variance may be due to the presence of multiple wing shape-variation modes within the female dataset. The small sample sizes available for this investigation prevent any definitive conclusions from being drawn with regard to the issue complex patterns of variation in female *C. bezziana* at this time. Nevertheless, it is abundantly clear that, within this dataset (1) there is a marked difference along PC-1 between female wings that project to intermediate and high positions along PC-2, (2) a marked difference between male and female

wings that project to high positions along PC-1 and (3) a small group of three (possibly four) female wings that exhibit anomalously low scores along PC-2. In future investigations it will be important to examine the question of whether these apparent distinctions are artifacts of a small sample size or represent a fundamental aspect of the morphological structure of female *C. bezziana* populations.

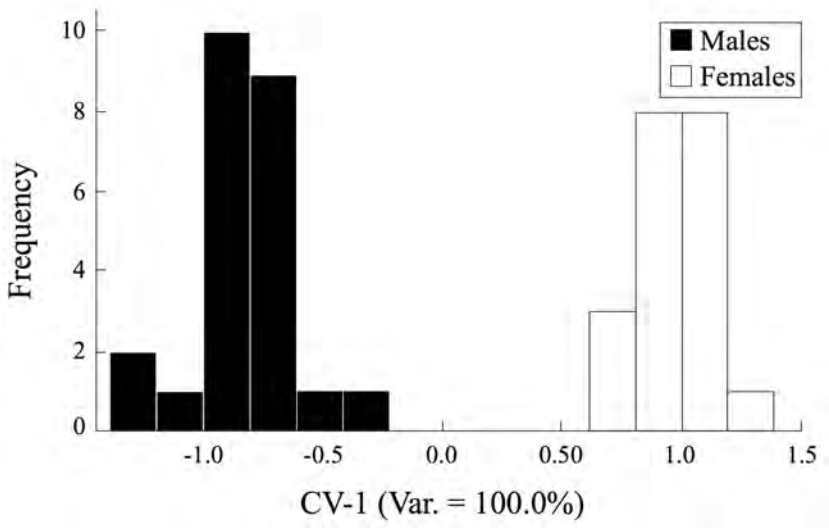


Figure 14. Frequency histogram of the projections of *C. bezziana* scores on PCs 1-27 onto the CVA discriminant axis separating Asian (Sumba) male and female populations. The between-groups separation is significant at the $\alpha < 0.01$ level as assessed by a bootstrap test of the log-likelihood ratio index.

As was the case with the previous geography-difference analysis, despite the apparent overlap between male and female Asian (Sumba) wing image configuration fields within the subspace formed by the first three pooled PCA axes (see Fig. 13), when the projected scores along all 27 eigenvector variables required to represent 95 percent of the pooled variation in image configurations are included, a CVA to test for gender differences, male and female wings are separated in markedly different and mutually exclusive shape-configuration fields along the single linear discriminant axis (Fig. 14). A non-parametric bootstrapped log-likelihood ratio test of group separation along this axis found that none of the 1,000 pseudoreplicate datasets created randomly from these data with replacement produced $\phi$-index values greater than 56.0 whereas the $\phi$-index value calculated for the gender-difference test was 94.3. Accordingly, this result is interpreted as being statistically significant at greater than the $\alpha = 0.01$ level.

In addition, despite the small size of this sample the CV-1 discriminant function exhibits very good stability with a jackknife (leave one out) analysis of post-hoc identification power returned a

result of 93.18 percent correct identifications for training set wings that were treated as unknown specimens and prevented from participating in estimating the discriminant function. Once again, the group with the largest sample size (males) exhibited the smallest number of misidentifications in this test, with one male specimen misidentified, post hoc, as female whereas two female specimens were misidentified as male.

In addition to answering the question of whether sexually dimorphic patterns of variation exist in these wing-image data, geometric morphometric approaches can also be used to reveal the specific aspects of wing morphology that vary between *C. bezziana* sexes and in which relative directions those variations occur. Figure 15 provides illustrates the reconstructed forms of typical male and female Asian (Sumba) *C. bezziana* wing morphologies at specific locations along the discriminant axis, along with a colour-coded image-difference map that highlights regions of pronounced sexually dimorphic distinction.

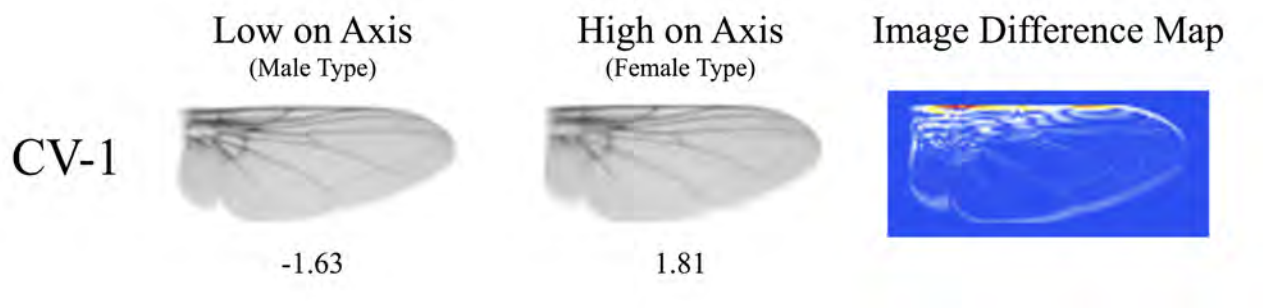


Figure 15. *Chrysomya bezziana* wing image models constructed at the ends of the distributions of image projections along the Asian (Sumba) male - female linear discriminant axis (CV-1). Distinctions between these images represent the major models of digital image distinction on a pixel-by-pixel basis. Numbers below the hypothetical image models represent the coordinate values at which the models were constructed. The final column contains a pixel difference maps in which the values of the differences between pixel brightness values have been colour-coded on a continuous scale as described in the Fig. 5 caption. See text for discussion.

Based on a detailed comparison of these images, and guided by the CV-1 image-difference map, the primary distinctions between male and female Asian (Sumba) *C. bezziana* wings fall into three regional categories. First and most important is an increase in the space between the costal margin and both the lateral segments of the subcostal and primary anterior radius veins in females relative to the distinctly more compact arrangement of these features in males. In the context of the images used in this investigation, this expansion or narrowing (depending on which sex is considered as the basal state) is manifested as a migration of the costal margin in an anterior direction with particularly intensive distinctions between pixel grayscale values occurring at the anterior terminus of the humeral transverse vein, the humeral articulation or break, and the anterior termini of the

subcostal, anterior radius and the first and second post-anterior radius veins. Coincident with this distinction between males and females in the leading wing edge, males also exhibit wings that are much more narrow distally than female wings. In terms of the images used in this investigation this apparent sex-linked variation manifests itself as an anterior migration of the posterior wing margin, especially in the middle region of the wing blade. This change also involves a more subtle anterior migration of the distal medial and medial-cubital transverse veins. In general, these changes can be summarized as an overall narrowing of the main wing blade in male Asian (Sumba) *C. bezziana* relative to the typical female condition which results in accentuating the ellipticity of the distal wing tip. Finally, the indentation in the posterior wing margin that marks the intersection between the anal alular regions is, on the whole, far more distinct and deeper in male, as opposed to typically female wings. In female *C. bezziana* the anal-alular indentation is, on the whole, shallower and much less pronounced.

It should be stressed that these are preliminary findings based on the detailed analysis of a relatively small sample. What can be said with confidence is that, based on these data, a clear potential exists to identify quite subtle aspects of blowfly biology from disjunct patterns of morphological variation that occur in aspects of the phenotype — such as the wing — that are readily accessible to monitors with only the most rudimentary training in specimen-handling procedures and blow fly taxonomy. Even more importantly, reliable identifications can made quickly, efficiently, and on a quantitative basis using appropriate morphometric procedures; procedures that can, at least in principle, be fully automated.

## Discussion

In the same way that mathematics can be defined as the study of patterns in numbers (Delvin, 1994; 1998; Gowers *et al*., 2008), natural history can be defined as the study of patterns in nature with a non-exclusive emphasis on their origin. This definition unites all attempts to study nature (biological and physical) in a manner that is consistent with the history of this field (see Jardine *et al*., 1996) and encompasses its discovery, descriptive (idiographic) and theoretical/conceptual (nomothetic) aspects. Such a formulation also emphasizes the utility and importance of mathematics in the investigation of natural history phenomena, a tool that has become increasingly important during its development over the last century (Sokal and Sneath, 1966; MacArthur and Wilson, 1967;

Blackith and Reyment, 1971; Sneath and Sokal, 1973; Reyment *et al*., 1984; Hull, 1988; Bookstein, 1991; McGhee, 1999; Sepkoski, 2002; Felsenstein, 2003; McGhee, 2007; Sokal and Rohlf, 2012).

The discipline — some prefer to call it a 'tool' — of morphometrics has been a prominent and highly successful example of this increasingly mathematical approach to the analysis of natural history phenomena (see Adams *et al*., 2004; Adams *et al*., 2013; MacLeod in press a; in press b). To date, applied morphometrics has been used to investigate a wide range of both intra-specific and inter-specific patterns, including growth and development (e.g., Klingenberg, 2016), evolutionary rates (e.g., Bookstein, 2012; Adams, 2014), modularity (e.g., Mitteröcker and Bookstein, 2007; Klingenberg 2013), comparative morphology (e.g., Felsenstein, 2002; MacLeod, 2002; Catalan *et al*., 2010; Globoff and Catalan, 2011; Klingenberg and Gidaszewski, 2010), and fluctuating asymmetry (e.g., Montiero, 2013; Polly *et al*., 2013). However, few results of investigations that seek to discriminate between different intra-specific and inter-specific groups of closely related species have been dramatically successful to date (e.g., Zelditch *et al*., 1995; Walker, 1996; Ibañez *et al*., 2007, but see MacLeod, 2002; 2015; MacLeod and Steart, 2015). Accordingly, we are unaware of the identification of any species that is undertaken primarily via reference to morphometric data or that has been automated to the extent that identification can be made reliably by non-expert taxonomists. Yet, the scientific community is agreed that its inability to obtain identifications of biological species (and other types of groupings) quickly, consistency and with a high degree of accuracy is a major impediment that not only limits the scope of scientific research, but has severe and costly economic and medical implications (Kaesler, 1993; MacLeod *et al*., 2010).

It is highly unlikely that the answer to this dilemma will be found in training up a new generation of taxonomists, either in principle (Godfray, 2002; Godfray *et al*., 2007) or in practice (Culverhouse *et al*., 2013). Use of DNA barcodes poses a practical means of addressing the need for reliable and consistent identifications in certain instances (e.g., for parts of specimens and/or in assays of species richness for which there is no opportunity and/or no need to recover whole specimen bodies). However, controversy continues to surround the routine use of DNA technology for species identification on a variety of fronts (Ebach and Carvalho, 2010; Jingo *et al*., 2011; Shen *et al*., 2013). Moreover, in the vast majority of instances, accurate identifications can be made as they always have been made, on the basis of morphological criteria alone — especially if the ability of humans to perceive such distinctions can be extended, speeded and made more objective via recourse to appropriate technologies. In other words, the application of morphometric data collection and analysis procedures to the automated identification of plant and animal groups

represents an outstanding opportunity for the biometric community; an opportunity with widely acknowledged to have important scientific, economic and social implications.

For the past 30 years landmarks and semilandmarks (= the serially arranged analogues of landmarks) have been the basic data of morphometrics and the foundation of the geometric morphometric approach (Kendall, 1984; Bookstein, 1986; 1991). However, Bookstein (2016) has recently argued that, in order to render morphometric results more compatible with process-level biological explanations, the fundamental symmetries of the standard morphometric data matrix are deficient in precisely the sort of information that is necessary — and in many cases readily available — to support this praxis between pattern and process. Landmark-based data matrices contain no information about natural aspects of variation among landmark locations which, in turn, reflect groupings between different developmental, functional, physiological or phylogenetic aspects of the organisms in question. Moreover, landmark-based datasets include only those features of the organism that can be reasonably well represented by the specification of a landmark, irrespective of whether such locations are known or suspected to be of importance to the resolution of the biological problem under investigation. In contrast, digital images of organismal bodies or structures of interest (e.g., insect wings) contain informative representations of all features that might conceivably be of interest in testing a biological hypotheses or characterizing a biological group and do so in a manner that is tractable in terms of standard matrix notation and that supports direct visualization/modelling.

By the same token, the standard decomposition of landmark-based morphometric data matrices via PCA, and the presentation of patterns of similarity and difference on ordination spaces derived from eigenvectors of the pooled shape covariance matrix, often fails to include any information about differences among groups known to reside within the sample. The orthogonality constraint enforced by an eigenanalysis of pooled-sample data guarantees that the resulting eigenvectors will specify sets of contrasts between landmark locations that ignore both the natural structure of groups among the landmark locations and the structure of groups among the specimens from which those data have been collected. Aspects of structures may be revealed by the PCA analysis of morphometric data, but only if they deterministically or coincidentally align with the major orthogonal directions of form/shape variation within the pooled-groups sample. Even if this alignment is present within a dataset it will rarely be the case that the full measure of group-level distinction will be able to be assessed via simple inspection of ordinations formed by form/shape configurations projected into low-dimensional spaces formed by the first few eigenvectors. As we can see from the detailed analysis of the geographic-difference *Chrysomya*-wing dataset presented

above, even in instances where this turns out to be the case in general, it is virtually always not the case in particular. Use of PCA to represent the structure of form/shape variation in a sample can only be justified biologically in the absence of any information about such natural groupings among the variables (= landmarks) and objects (= specimens) in question or in the event that the major directions of pooled group variation happen to coincide with between variable-group and between-specimen group contrasts.

In order to address this data analysis problem Mitteröcker and Bookstein (2014, see also Bookstein 2016, Flury 1983, 1985) have advocated use of relative principal component analysis ($PCA_r$) or relative eigenanalysis in order to include information about the presence of, and structure of relations between, biological groups residing within morphometric datasets. These relative principal components provide an indication of the difference in structure between two or more group-specific covariance matrices as a series of vectors whose directions and lengths have been adjusted to reflect the ratios of the original variables along with all their linear combinations. Under this model, normal PCA can be regarded as the outcome of a relative eigenvector analysis in which the covariance matrix of the second (non-present) group is represented by the identity matrix (= unit variance for all variables and no covariance between all pairs of different variables). Mitteröcker and Bookstein (2014) provide equations for calculating the relative eigenvectors of any two groups as a contrast between their covariance matrices. These authors also note that CVA is equivalent to a $PCA_r$ under the assumption that the covariance matrices are equivalent across all groups, though it is actually the projection of the CVA eigenvectors into the space of the original variables that constitutes the relative principal components. This can appreciated insofar as CVA eigenvectors are orthogonal to one another in the CVA space, but not in the space of the space of the original variables. Regardless, so long as it is born in mind that, unlike normal PCA eigenvectors, $PCA_r$ eigenvectors define a space in which the axes are non-orthogonal and aligned with the directions group-level contrasts, the inspection, analysis and modeling of point locations within the $PCA_r$ space can be both interesting and informative.

Inspecting results of the CVA for all three of our test datasets (see figs 4, 8, 11 and 14) all groups appear to have quite similar variance representations within the canonical variate space. Accordingly, results obtained from this investigation can not only be regarded as constituting valid representations of group differences, but of also of group-level contrasts, especially if back-projected into the space of the original variables and used to assess the directions of maximal group contrast. This is precisely the procedure that was used in the present analysis to obtain the pixel-based, image-difference maps for the geographic, gender, and species-difference tests (see figs 9, 12

and 15; see also MacLeod 2015 for another example of this visualization procedure). In other words, by employing a CVA of PCA score data it is not only possible to calculate and portray the major directions of between-group differences within a $PCA_r$-like space as scatterplots of points, the entire $PCA_r$ ordination space can be used as a mathematical platform from which visualisations of the geometric meaning of $PCA_r$ axes can be created. Mitteröcker and Bookstein (2014, see also Bookstein, 2016) explain how this procedure can work with traditional multivariate morphometric and geometric morphometric data. The present study extends this formalism to a direct analysis of digital images — a form of morphometric data that has been little used by morphometricians thus far, but that is coming to be recognized as having many innate advantages over traditional landmark/semilandmark data.

Of course, the implications of using digital images themselves as the subjects of morphometric analyses transcends both biology and natural history. The formalism of having to represent objects of interest via recourse to landmark configurations and/or sets of serially arranged semilandmarks imposes severe limitations on the range of subjects considered amenable to morphometric analysis, on the scope of investigations that could be carried out using a collection of specimens or objects, and on the acuity of hypotheses that can be considered using geometric morphometric approaches. The labour needed to collect even small suites of landmarks, one-at-a-time, by hand, also exerts a considerable constraint on the size of morphometric datasets that can be assembled practically and, so, on the accuracy of statistical tests based on morphometric data. Moving from a consideration of geometric variations between landmarks to a geometric consideration of pixels in the frame of a digital image not only means that greater amounts of data can be collected for morphometric analysis quickly, efficiently, and in a wide variety of laboratory and field contexts, it also means that new aspects of specimen/object morphology can be included in any morphometric investigation (e.g., variable colour and texture patterns, such as damselfly wing spots – Upton *et al*., 2016).

Along with these new capabilities, however, comes a new range of data-collection concerns that morphometricians who wish to undertake the direct analysis of images will need to develop strategies to cope with and overcome. Because landmark data capture no information about the image itself, images of widely varying formats, resolutions, colors and illumination modes may be used in morphometric analysis. But in order to be useful in any image-based analysis all of these parameters must be standardized. In addition, specimens must be inspected carefully for any systematic differences that are not part of the inherent biological or physical aspect of the specimens of interest. For example, specimens of different ages in museum collections, or those that have been subjected to different processing procedures, may be darker or exhibit a different color or tint

relative to other specimens in the collection. As any aspect of the image that causes alteration of the pixel color and /or brightness values can affect the images' covariance with other images in the sample, only those that reflect the normal ranges of natural variation should, ideally, be used in image-based morphometric analyses. In some cases, the influence of exogenous sources of image variation may be minimized via the application of various image-processing procedures (e.g., alterations in color patterns can be minimized by converting the images to a grayscale colour mode prior to analysis, non-biological variations in brightness or darkness values may be normalized via adjustments of the image histogram). In others this difficulty may be able to be overcome during the data-analysis phase of the investigation (e.g., via employment of machine learning procedures, see MacLeod *et al*., 2007a; 2007b; 2015b; in press). Regardless, care must be taken to collect images using standardized procedures at the outset of any analysis. In addition, if automated specimen identification is the goal of the analysis, care must be taken to collect training set images using image-capture equipment and under illumination conditions that can be reproduced in remote laboratories and/or in the field.

This having been said, the amount of information residing within digital images is sufficiently large that imperfect specimens can often be used to construct training sets and obtain identifications. Missing data has been a long-standing issue in geometric morphometrics insofar as there it is difficult to locate a landmark or semilandmark at a position corresponding to an aspect of an organismal body that is not present or that has been obscured in any way (see Strauss *et al*., 2003; Strauss and Atabassov, 2006; Brown *et al*., 2014). Several procedures have been developed to meet surmount this challenge in particular instances (e.g., Clavel *et al*., 2014; Arbour *et al*., 2014). Under the direct image analysis approach, however, similarity and difference estimates are based on the total set of pixels comprising the image — even in the cases where the dimensionality of the image data has been reduced via PCA. As a result, relatively minor, localized imperfections in the specimen included in a sample are usually insufficient to cause major perturbations in the structure of either pooled or group-specific image covariance matrices. Moreover, there is usually little need to employ special procedures to cope with such imperfections so long as the major characteristics of the specimen or structure in questions are retained. Indeed, stepping the image resolution down to a relatively low value in order to address the pixel-value redundancy issue often has the effect of minimizing the influence of minor, localized imperfections such to the point that these play little on no role in determining the result of an image-based morphometric analyses (see Fig. 2). Large or generalized deformations of the specimen — and so the specimen's digital image — can be problematic. But even in these cases the higher information content of images, coupled with either

the smoothing effect of resolution reduction prior to PCA/CVA analyses or the use of robust machine-learning procedures, can mitigate the effects of imperfections that would render a specimen unsuitable for inclusion in a traditional landmark-based morphometric sample.

Close inspection of the images used in this investigation (see supplementary data) will show that many contain minor imperfections such as tears in the wing membrane, dust particles in the image frame, variable degrees of overlap between the anal and alular areas of the wing blade, variable degrees of wing darkening, and variable degrees of pigmentation of the pteralia or auxiliary area along with a wide range of variable damage at the base where the wing has been detached from the specimen's body. None of these sources of variation were sufficient to mask the clear and statistically significant differences found between *Chrysomya* species, geographic populations or genders.

In addition, the direct analysis of images in a quantitative geometric context represents the critical link between the heretofore separate fields of morphometrics and computer vision. Conceptually, the growing field of computer vision overlaps strongly with that of morphometrics insofar as both involve the acquisition, processing, analysis and understanding of images. In the case of morphometrics images are regarded as representing a proxy for the specimen or set of specimens under consideration. But in the vast majority of cases both landmarks and semilandmarks are acquired from 2D or 3D digital representations (= digital images) of these specimens rather than from the specimens themselves.

Computer vision and morphometrics have different origins and were developed in different contexts to meet different needs. To date there has been minimal crossover between these fields. Nevertheless, their ultimate goals of extracting information from images that is pertinent to understanding the world around us is very similar. Both could — and in some cases do — take advantage of developments and discoveries made in the other field. The purpose of both Sirovich and Kirby's (1987) and Turk and Pentland's (1991) original application of PCA to digital images was to facilitate the automated identification of human faces for the purpose of developing computer vision procedures. Similarly, image keypoints (see Lowe, 1999; 2004; Key *et al*., 2004) represent a generalized and mathematically sophisticated attempt to algorithmically identify and operate on corresponding landmark locations in two or more images - a procedure morphometricians are very familiar with but, at the moment, are forced to do by hand. Computer-vision specialists recognize the value of being able to locate topologically corresponding landmark locations that make sense in various contexts (e.g., functional, phylogenetic, ecological). For the most part, however, they lack the understanding of these contexts necessary to build this capability

into their image-processing algorithms. Similarly, the form/shape modelling aspects of morphometric techniques that have been developed by morphometricians and that have become so important in enhancing the interpretability of morphometric analyses are, if anything, under-appreciated by computer-vision researchers. Perhaps most importantly, practitioners in both fields are increasingly coming to realize that the real purpose of morphometrics and computer vision is not to be found in the development of algorithms, image processing procedures or data analysis techniques, but rather in the practical uses to which such information can be put to solve real-world problems. The *Chrysomya* study presented above represents an example of how these two fields can be brought together in ways that lead to increased scientific understanding of variation in natural populations.

Of course, an obvious additional implication of our findings is that, by using the methods we have employed, it may now be possible to produce a much-needed, accurate and inexpensive fully automated software tool that can be used by a wide variety of groups (e.g., agriculturalists, medical researchers, epidemiologists, ecologists and taxonomists) to support a wide range of quick, easy and accurate identifications of importance in economic, human health and biological contexts. Based on the results we have obtained in the course of this study, the potential of a digital image-based approach to the practical investigation and analysis of the natural world seems clear and its scope virtually unlimited.

## Conclusions

The ability to make routine, automated identifications of the Old World screwworm fly species *C. bezziana* and its relatives would be beneficial in a wide variety of scientific, medical, forensic, and agricultural contexts. While DNA barcoding could be employed for this purpose in principle, a more efficient, practical, rapid, and in many ways interesting approach to this problem would be to identify a morphological character complex with sufficiently well-structured patterns of variation to support automated or quasi-automated identification, especially if such identification systems could be located in the field and employ widely available technology (e.g., smartphone cameras). Based on results obtained from our investigation of African and Asian (Sumba) *Chrysomya* species it is clear that the morphology of the wing may represent such a character complex.

Analyses of a small sample of isolated wing images from C. *bezziana*, *C. megacephala*, and *C. rufifacies* has shown that this appendage not only contains sufficiently well-structured variation to

distinguish between these three species to a better than 90 percent accuracy level, but that similar analyses can also distinguish between Asian and African (Sumba) populations of C. *bezziana* and between the genders of this species. These identification accuracy ratios were obtained via the direct analysis of digital wing images with minimal image pre-processing and on wings that included a wide variety of imperfections. All statistical test results were significant as assessed using nonparametric bootstrap versions of standard discriminant analysis tests and all identification accuracy ratios were generated using robust, jackknife (leave-one-out) test procedures. Our image-based approach avoids the laborious and time-consuming need for trained taxonomists and/or parataxonomists to take specimens to a laboratory equipped with specialist image-analysis software in order to collect landmark and/or semilandmark data for geometric morphometric analysis. Moreover, the results obtained from our training set sample provide indications of between-group differences that might even allow such identifications to be made visually via simple inspection.

A landmark analysis of the wings used in the geographic population difference test confirmed the existence of differences between African and Asian (Sumba) wing morphologies — thus also confirming the appropriateness of the image-based results — and returned a marginally higher population identification accuracy ratio. However, the ease, speed, and convenience of the analysis of wing images directly, along with the high identification accuracy ratios achieved by our investigation, lead us to conclude that this strategy would be sufficient to provide field taxonomists, forensic researchers, medical specialists and agricultural workers with a reliable indication of species identity, population of origin and gender in the field. If more accurate identifications are needed and would be cost-effective, these could be generated by specialists in adequately equipped research laboratories on morphometric discrimination systems trained using traditional landmark/semilandmark data from the same set of wings used to train the direct image analysis system.

With regard to the larger implications of the approach to morphometric analysis we have taken, our study occupies the nexus between geometric morphometrics and computer vision. Our primary goals for this investigation were resolutely biological and, owing to the complex vein patterns that characterize insect wings, focused on structures which have been classic subjects for landmark-based geometric morphometrics (e.g., Rohlf, 1993). Our overall data-analysis procedure was also identical to that used in a standard geometric morphometric analysis whose purpose is to distinguish between groups. But rather than base our analysis on the spatial configurations of a relatively small number of landmark or semilandmark locations selected at the outset of our analysis, we chose to adopt a more exploratory strategy that did not require any *a priori* decisions to be made regarding what aspects of the wing may, or may not, be important sources of structured covariation that

characterize the different specimen groups. The digital images of insect wings that were used in our investigation captured all the biologically relevant morphological information available in our sample of wing specimens and used the totality of this information as the basis for our analysis. This approach to morphometric investigation is consistent with the spirit, if not entirely with the letter, of recent criticisms made by Bookstein (2016) regarding the appropriateness of standard geometric morphometric data and procedures for characterizing and resolving questions pertaining to biological hypotheses. But even more than this, the productive cross-fertilization that can exist between image-based morphometrics and image-based computer vision, as hinted at by Bookstein (2016), and as demonstrated by our results, provide a clear signpost pointing in the direction both fields may want to move in the future.

Geometric morphometrics can bring to complex biological issues an elegant and mathematically rigorous understanding of form variation along with a wide variety of tools through which the geometric implications of quantitative morphological data analyses can be portrayed in a manner that is both natural and easy to understand. But the methods employed in this field at present are not able to take adequate advantage of a wide variety of biological data that could, and we believe should, be included in the biological morphometric analyst's toolkit, along with an overall approach to analysis that is more confirmatory than exploratory in character. Computer vision can bring a far more extensive and mathematically sophisticated array of data and data-analysis tools to the classic problems posed by morphological variation. Nevertheless, the methods employed by this field, to date, lack an appreciation for the special character of biological data (e.g., the fact that all biological observations are embedded causally within a phylogenetic hierarchy and that biologically informative comparisons among organisms are best made accordingly to the principles of biological homology insofar as possible) and, in many instances, have been employed in the context of underdeveloped results-visualization tools. Both fields have much to learn from each other. But irrespective of these considerations, we expect results similar to those we have detailed above will likely be obtained from any investigation of other insect groups via the direct analysis of digital images of bodies and/or parts thereof and, indeed, from subjecting a wide variety of images of other plant, animal, and physical object groups to similar analyses.

## Acknowledgements

We would like to thank The Natural History Museum (London) and Indonesian Research Center for Veterinary Science for supporting this research and providing funding to continue our collaboration in this area. We are grateful to Burgert Muller, Ros Urban and Erica McAlister for enabling us to study specimens of *Chrysomya bezziana* from the collections of the Natal Museum, the National Collection of Insects, Pretoria (both in South Africa) and the Natural History Museum, London, respectively. We are also grateful to the International Atomic Energy Agency (IAEA, Austria; TC14842 and RC14860) for funding the insect collecting in Indonesia. All image processing operations were performed with Wolfram *Mathematica* software written for this project by the senior author. All data analyses were performed using image processing, image alignment, principal components analysis, canonical variates analysis, and statistical testing software also written by the senior author in *Mathematica.* All *Mathematica* notebooks used in this investigation are available from the corresponding author on request.

## References

Adams, D. C. 2014. Quantifying and comparing phylogenetic evolutionary rates for shape and other high-dimensional phenotypic data. *Systematic Biology*, **63**(2),166-177.

Adams, D. C., Rohlf, F. J. and Slice, D. E. 2004. Geometric morphometrics: ten years of progress following the 'revolution'. *Italian Journal of Zoology*, **71**(1), 5-16.

Adams, D. C. Rohlf, F. J. and Slice, D. E. 2013. A field comes of age: geometric morphometrics in the 21st century, *Hystrix*, **24**(1), 13-20.

Arbour, J. H., Brown, C. M. and Nakagawa, S. 2014. Incomplete specimens in geometric morphometric analyses. *Methods in Ecology and Evolution*, **5**(1),16-26.

Becerra, J., 1996. Imagina: A direct tool for image analysis in systematics, *in* Marcus, L. F., Corti, M., Loy, A., Naylor, G. J. P., and Slice, D., eds., *Advances in Morphometrics*. New York, Plenum Press, p. 83–90.

Becerra, J. M., Bello, E. and Garcia-Valdecasas, A. 1993. Building your own machine image system for morphometric analysis: A user point of view, *in* Marcus, L. F., Bello, E., and García-Valdecasas, A., eds., *Contributions to Morphometrics*. Madrid, Monografias del Museo Nacional de Ciencias Naturales 8, p. 65–92.

Blackith, R. E. and Reyment, R. A. 1971. *Multivariate morphometrics*, London, Academic Press, 412 p.

Bookstein, F. L. 1986. Size and shape spaces for landmark data in two dimensions. *Statistical Science*, **1**(2), 181-242.

Bookstein, F. L. 1989. Principal warps: thin-plate splines and the decomposition of deformations. IEEE Transactions on Pattern Analysis and Machine Intelligence, **11,** 567–585.

Bookstein, F. L. 1991. *Morphometric tools for landmark data: geometry and biology*, Cambridge, Cambridge University Press, 435 p.

Bookstein, F. L. 2012. Random walk as a null model for high-dimensional morphometrics of fossil series: geometrical considerations, *Paleobiology*, **39**(1), 52-74.

Bookstein, F. L. 2016. The inappropriate symmetries of multivariate statistical analysis in geometric morphometrics. *Evolutionary Biology* **43**, 1–37.

Brown, C. M., Arbour, J. H. and Jackson, D. A. 2012. Testing of the effect of missing data estimation and distribution in morphometric multivariate data analyses. *Systematic Biology*, **61**(6), 941–954.

Catalano, S. A., Goloboff, P. A. and Giannini, N. P.. 2010. Phylogenetic morphometrics (I): the use of landmark data in a phylogenetic framework. *Cladistics* **26**, 539–549.

Chesters, D., *et al*. 2012. The integrative taxonomic approach reveals host specific species in an encyrtid parasitoid species complex. *PLoS One*, **7**(5), e37655.

Clavel, J., Merceron, G. and Escarguel, G. 2014. Missing data estimation in morphometrics: how much is too much?. *Systematic Biology*, **63**(2), 203–218.

Comstock, J. H. and Needham, J. G. 1898. The wings of insects. *American Naturalist*, **33**, 117–126.

Culverhouse, P. F., *et al*. 2013. An empirical assessment of the consistency of taxonomic identifications. *Marine Biology Research*, **10**(1), 73-84.

Devlin, K. J. 1994. *Mathematics: the science of patterns - the search for order in life, mind and the universe*, New York, Scientific American Library, 216 p.

Devlin, K. J. 1998. *The language of mathematics: making the invisible visible*, New York, W. H. Freeman & Company Ltd., 300 p.

Ebach, M. C. and Carvalho, M. R. d. 2010. Anti-intellectualism in the DNA Barcoding Enterprise. *Zoologia (Curitiba, Impresso)*, **27**(2), 165-178.

Felsenstein, J. 2002. Quantitative characters, phylogenies, and morphometrics. *In* MacLeod, N. and Forey, P. L. eds. *Morphology, shape and phylogeny*. London,Taylor & Francis, p. 27–44. .

Felsenstein, J. 2003. *Inferring phylogenies*, Sunderland, Massachusetts, Sinauer Associates, 664 p.

Goloboff, P. A. And Catalano, S. A.. 2011. Phylogenetic morphometrics (II): algorithms for landmark optimization *Cladistics* **27**(1), 42–51.

Godfray, H. C. J. 2002. Challenges for taxonomy. *Nature*, **417**(2), 17–19.

Godfray, H. C., *et al*. 2007. The web and the structure of taxonomy. *Systematic Biology*, **56**(6), 943-955.

Gowers, T., Barrow-Green, J. and Leader, I. 2008. *The Princeton companion to mathematics*, Princeton, New Jersey, Princeton University Press, 1056 p.

Hall, M. J. R., MacLeod, N. and Wardhana, A. H. 2014. Use of wing morphometrics to identify populations of the Old World screwworm fly, *Chrysomya bezziana* (Diptera: Calliphoridae): a preliminary study of the utility of museum specimens. *Acta Tropica,* **138** Supplement, 49–55.

Hall, M. J. R., Wall, R. L and Stevens, J. R. 2016. Traumatic myiasis – a neglected disease in a changing world. *Annual Review of Entomology*, **61**, 159-176.

Hendrichs, J., *et al*. 2015. Resolving cryptic species complexes of major tephritid pests. *Zookeys*, **540**, 5-39.

Hull, D. L. 1988. *Science as a process: an evolutionary account of the social and conceptual developments in science*, Chicago, University of Chicago Press, 586 p.

Ibañez, A.L., Cowx, I.G., O'Higgins, P. 2007. Geometric morphometric analysis of fish scales for identifying genera, species, and local populations within the Mugilidae. *Canadian Journal of Fisheries and Aquatic Sciences* **64**, 1091-1100.

Irish, S. Lindsay, T. Wyatt, N. 2014. Key to adults of Afrotropical species of the genus *Chrysomya* Robineau-Desvoidy (Diptera: Calliphoridae). *African Entomology*, **22**, 297-306.

Ke, Y. and Sukthankar, R. 2004. PCA-SIFT: a more distinctive representation for local image descriptors, *In Proceedings of the 2004 IEEE Computer Society Conference on Computer Vision and Pattern Recognition*, IEEE Computer Society, Washington, D.C., p. 506–513.

Kendall, D. G. 1984. Shape manifolds, procrustean metrics and complex projective spaces. *Bulletin of the London Mathematical Society*, **16**, 81–121.

Jardine, N., Secord, J. A. and Spary, E. C. 1996. *Cultures of natural history*, Cambridge, Cambridge University Press, 501 p.

Jinbo, U., Kato, T. and Ito, M. 2011. Current progress in DNA barcoding and future implications for entomology. *Entomological Science,* **14**(2), 107-124.

Johnson, N., and Triplehorn, C. A. 2005. *Borror and Delong's introduction to the study of insects*, 7th edition, Detroit, Michigan, Cengage, 888 p.

Kaesler, R. L. 1993. A window of opportunity: peering into a new century of paleontology. Journal of Paleontology, 67, 329–333.

Ke, Y., Sukthankar, R., 2004. PCA-SIFT: a more distinctive representation for local image descriptors. IEEE Computer Society, Proceedings of the 2004 IEEE Computer Society Conference on Computer Vision and Pattern Recognition, pp. 506–513.

Klingenberg, C. P. 2013. Cranial integration and modularity: insights into evolution and development from morphometric data. Hystrix, 24(1), 49-64.

Klingenberg, C. P. 2016. Size, shape, and form: concepts of allometry in geometric morphometrics: *Development, Genes and Evolution*, 226(3), 113–137.

Klingenberg, C. P. and Gidaszewski, N. A. 2010. Testing and quantifying phylogenetic signals and homoplasy in morphometric data. Systematic Biology, **59**(3), 245-61.

Lowe, D. G. 1999. Object recognition from local scale-invariant features, *In Proceedings of the 7th IEEE International Conference on Computer Vision*, Corfu, Greece, Volume 2, p. 1150–1157.

Lowe, D. G. 2004. Distinctive image features from scale-invariant keypoints. *International Journal of Computer Vision*, **60**(2), 91–110.

MacArthur, R. H. and Wilson, E. O. 1967. *The theory of island biogeography*, Princeton, Princeton University Press, 203 p.

MacLeod, N. 1990 Digital images and automated image analysis systems, *in* Rohlf, F. J., and Bookstein, F. L., eds., *Proceedings of the Michigan Morphometrics Workshop*, Volume Special Publication no. 2: Ann Arbor, Michigan, The University of Michigan Museum of Zoology, Special Publication 2, p. 21-35.

MacLeod, N. 2002. Phylogenetic signals in morphometric data. *In* MacLeod, N. and Forey, P. L. eds., *Morphology, shape and phylogeny*. London, Taylor & Francis, p. 100–138. .

MacLeod, N. 2007a. *Automated taxon identification in systematics: theory, approaches, and applications*, London, CRC Press, Taylor & Francis Group, 339 p.

MacLeod, N. 2007b. Groups II. *Palaeontological Association Newsletter*, **65**, 36–49.

MacLeod, N., Benfield, M., and Culverhouse, P. F. 2010. Time to automate identification. *Nature*, **467**(9), 154–155.

MacLeod, N. 2014. Imaging and analysis of skeletal morphology: new tools and techniques. *In:* Metcalfe, R. J., Crockitt, J. A. & David, A. R. (eds) *Palaeopathology in Egypt and Nubia: a century in review.* Oxford: Archaeopress.

MacLeod, N. 2015a. The direct analysis of digital images (eigenimage) with a comment on the use of discriminant analysis in morphometrics, *in* Lestrel, P. E., (ed.), *Proceedings of the Third International Symposium on Biological Shape Analysis*. Singapore, World Scientific, p. 156–182.

MacLeod, N. 2015b. A comparison of alternative form-characterization approaches to the automated identification of biological species, in, Hamilton, A., (ed.) *Evolution of phylogenetic systematics*. Berkeley, California, University of California Press, p. 214–245.

MacLeod, N. in press a. Morphometrics: history, development methods and prospects. Zoological Systematics.

MacLeod, N. in press b. On the use of machine learning methods in morphometric analysis. in Lestrel, P. E. (ed.), *Proceedings of the Fourth International Symposium on Biological Shape Analysis*. Singapore, World Scientific.

MacLeod, N., Krieger, J. and Jones, K. E. 2013. Geometric morphometric approaches to acoustic signal analysis in mammalian biology. *Hystrix*, **24**(1), 116-125.

MacLeod, N., O'Neill, M. A. and Walsh, S. A.. 2007a. A comparison between morphometric and artificial neural net approaches to the automated species-recognition problem in systematics, *in* Curry, G. and Humphries, C. (eds). *Biodiversity databases: techniques, politics, and applications*. Boca Raton, Florida, CRC Press, Taylor & Francis Group, p. 37–62.

MacLeod, N., O'Neill, M. A. and Walsh, S. A.. 2007b. Automated tools for the identification of taxa from morphological data: face recognition in wasps, in MacLeod, N., ed., *Automated taxon recognition in systematics: theory, approaches and applications*. Boca Raton, Florida, CRC Press, Taylor & Francis Group, p. 153–188.

MacLeod, N. and Steart, D. 2015. Automated leaf physiognomic character identification from digital images. *Paleobiology*, **41**(4), 528–553.

McGhee, G. R., Jr. 1999. *Theoretical morphology: the concept and its applications*, New York, Columbia University Press, 316 p.

McGhee, G. R. 2007. *The geometry of evolution: adaptive landscapes and theoretical morphospaces*, Cambridge, Cambridge University Press 216 p.

Manly, B. F. J. 2006. *Randomization, bootstrap and Monte Carlo methods in biology*, third edition. Chapman Hall/CRC, Boca Ration, Louisiana, 480 p.

Mitteröcker, P. and Bookstein, F. L. 2007. The conceptual and statistical relationship between modularity and morphological integration. *Systematic Biology*, **56**, 818–836.

Monteiro, L. R. 2013. Morphometrics and the comparative method: studying the evolution of biological shape. *Hystrix*, **24**(1), 31-38.

Morgan, A. H. 1912. Homologies in the wing-veins of mayflies. *Annals of the Entomological Society of America*, **5**, 89–106.

Pimentel, R. A. 1979. *Morphometrics: the multivariate analysis of biological data*, Dubuque, IA, Kendall/Hunt, 275 p.

Polly, P. D., *et al*., 2013, Phylogenetic principal components analysis and geometric morphometrics. *Hystrix*, **24**(1), 39-47.

Quezada-Euán, J. J. G., *et al*. 2015. Identification of cryptic species and morphotypes in male *Euglossa*: morphometric analysis of forewings (Hymenoptera: Euglossini). *Apidologie*, **46**(6), 787-795.

Reyment, R. A., Blackith, R. E. and Campbell, N. A. 1984. *Multivariate morphometrics* (second edition), London, Academic Press, 231 p.

Rohlf, F. J. 1993. Relative warp analysis and an example of its application to mosquito wings, *in* Marcus, L. F., Bello, E., and García-Valdecasas, A., eds., *Contributions to morphometrics*. Madrid, Museo Nacional de Ciencias Naturales **8**, 131–160.

Sepkoski, D. 2012. *Rereading the fossil record: the growth of paleobiology as an evolutionary discipline*, Chicago, London, The University of Chicago Press, 440 p.

Shen, Y. Y., Chen, X. and Murphy, R. W. 2013. Assessing DNA barcoding as a tool for species identification and data quality control. *PLoS One*, **8**(2), e57125.

Sirovich, L., and M. Kirby. 1987. Low-dimensional procedure for the characterization of human faces. Journal of the Optical Society of America, **A4**(3), 519–524.

Sokal, R. R. and Rohlf, F. J. 2012. *Biometry*, 4th edition, New York, W. H. Freeman and Company, 937 p.

Sokal, R. R. and Sneath, P. A. 1963. *Principles of numerical taxonomy*, San Francisco, W. H. Freeman, 359 p.

Sneath, P. H. A. and Sokal, R. R. 1973. *Numerical taxonomy: the principles and practice of numerical classification*, San Francisco, W. H. Freeman, 573 p.

Strauss, R. E., Atanassov, M. N. and De Oliveira, J. A. 2003. Evaluation of the principal-component and expectation-maximization methods for estimating missing data in morphometric studies. *Journal of Vertebrate Paleontology*, **23**(2), 284-296.

Strauss, R. E., and Artanassov, M. N. 2006. Determining best complete subsets of specimens and characters for multivariate morphometric studies in the presence of large amounts of missing data. *Biological Journal of the Linnean Society,* **88**, 309–328.Sulston, E.C.J., Wardhana, A.H., Hall, M.J.R., Logan, J.G., Gezan, S.A. and Cameron, M.M. 2014. Combining cattle and wound-

derived synthetic attractants, POC and Bezzilure, for sampling *Chrysomya bezziana* in Indonesia. *Acta Tropica* **138S**, S69-S75.

Sukontason, K. L., Narongchai, P., Sripakdee, D., Boonchu, N., Chaiwong, T., Ngern-klun, R., Piangjai, S. and Sukontason, K. 2005. First report of human myiasis caused by *Chrysomya megacephala* and *Chrysomya rufifacies* (Diptera: Calliphoridae) in Thailand, and its implication in forensic entomology. *Journal of Medical Entomology* **42**, 702-704.

Turk, M. and Pentland, A. 1991. Eigenfaces for recognition. *Journal of Cognitive Neurosciences*, **3**(1), 71-86.

Upton, L., Price, B., Percy, D., and Brooks, S. 2016. Applying novel digital visualization tools and traditional morphometrics to the analysis of wing size and asymmetry and to male wing spot size in *Calopteryx splendens* (Harris) (Banded Demoiselle). *Journal of the British Dragonfly Society* **32**, 8-25.

Walker, J. A. 1996. Ontogenetic allometry of threespine stickleback body form using landmark based morphometrics. *In* Marcus, L.F., Bello, E., García-Valdecasas, A. (Eds.), Contributions to morphometrics. Madrid, Museo Nacional de Ciencias Naturales 8, p. 193–214.

Zelditch, M. L., Fink, W. L., and Swiderski, D. L. 1995. Morphometrics, homology, and phylogenetics: quantified characters as synapomorphies. *Systematic Biology* **44**, 179–189.

Figure Captions

Figure 1. Morphology (A) and landmark-based sampling (B) of the *Chrysomya* wing. Morphological characters included the following humerus-radius articulation (H-RA), humerus-costa transverse vein (H-CT), costal margin (C), subcostal vein (SC), anterior radius vein (AR), first post-anterior radius vein (PA1R), second post-anterior radius vein (PA2R), wing tip (Tip), medial vein (M), radius-medial transverse vein (R-MT), cubital vein (Cu), proximal medial-cubital transverse vein (M-CT1), distal medial-cubital transverse vein (M-CT2), distal anal vein (A1), proximal anal vein (A2), cubital-distal anal transverse vein, alulal-anal indentation (Al-An). Landmarks: 1 - intersection between the humeral transverse vein and costal vein, 2 - position of the humeral articulation or break, 3 - intersection between the subcostal and costal veins, 4 - intersection between the anterior branch of the anterior radius vein (AR) and the costal margin (C), 5 - intersection between the first post-anterior branch of the radius vein (PA1R) and the costal margin (C), 6 - intersection between the second post-anterior branch of the radius vein (PA2R) and the costal margin (C), 7 - intersection between the medial vein (M) and the costal margin (C) or wing periphery, 8 - intersection between the cubital vein (Cu) and wing periphery, 9 - distal intersection between the anal and alulal areas (Al-Au), 10 - articulation between the humeral sclerite and the radius vein (H-RA), 11 - first bifurcation of the radius vein (AR) resulting the creation of this vein's anterior (AR) and first post-anterior (PA1R) branches, 12 - second bifurcation of the radius vein (AR) resulting the creation of this vein's first post-anterior (PA1R) and second post-anterior (PA2R) branches, 13 - anterior intersection between the radius-medial transverse vein (R-MT) and the second post-anterior radius vein (PA2R), 14 - anterior intersection between the distal medial-cubital transverse vein (M-CT1) and the medial vein (M), 15 - posterior intersection between the radius-media transverse (R-MT) vein and the medial vein (M), 16 - anterior intersection between the distal medial-cubital transverse vein (M-CT2) and medial vein (M), 17 - maxima of curvature in the distal portion of the medial vein (M), 18 - bifurcation between the cubital (Cu) and first anal (A1) veins, 19 - posterior intersection between the proximal medial-cubital transverse vein (M-CT1) and the cubital vein (Cu), 20 - posterior intersection between the proximal medial-cubital transverse vein (M-CT2) and cubital vein (CU), 21 - posterior intersection between the cubital-first anal transverse vein (C-AnT) and the first anal vein (A1). Specimen shown is BMNH E 1195306 which is a female African *C. bezziana*.

Figure 2. Original (upper row) and reduced resolution grayscale digital images of representative female specimens of the three species considered in this investigation.

Figure 3. Projection of the *C. bezziana* Procrustes-aligned, wing landmark configurations into the space formed by the first three principal components of the shape covariance matrix. This subspace represents c. 50% of the shape variation recorded by these landmarks. Note strong separation between African and Asian populations within the PC-1 vs. PC-2 subspace and lack of obvious shape outliers.

Figure 4. Frequency histogram of projected *C. bezziana* wing landmark configurations on the CVA discriminant axis separating African and Asian (Sumba) populations. This between-groups separation is significant at the $\alpha < 0.01$ level as assessed by a bootstrap test of the log-likelihood ratio index.

Figure 5. Directions of landmark migration between typical African (landmark configuration and displacement vector tails) and Asian (displacement vector heads) wings. See Fig. 1 for landmark names and defining criteria. The length of these vectors has been exaggerated (x3) in order to illustrate their directions and relative magnitudes. In addition, the landmark icons have been colour-coded to classify them into relative change categories: blue - no or small change, white - moderate change, yellow and orange - strong change, red - strongest change. See text for discussion.

Figure 6. Projection of the African and Asian (Sumba) *C. bezziana* major axis-aligned, wing image configuration data into the subspace formed by the first three principal components of the image covariance matrix. This subspace represents c. 60% of the shape variation recorded by the reduced resolution wing images. Note strong, but not perfect, separation between African and Asian (Sumba) populations within the PC-1 vs. PC-2 subspace, presence of several morphological subclusters, and presence of obvious shape outliers.

Figure 7. *Chrysomya bezziana* wing image models constructed at the ends of the of the distributions of image projections along each of the first three principal components of the image covariance matrix for the pooled (African-Asian [Sumba]) wing image data. Distinctions between these images represent the major modes of image variation on a pixel-by-pixel basis. Numbers below the hypothetical image models represent the coordinate values at which the models were constructed. The final column contains image difference maps in which the values of the differences between pixel brightness values have been colour-coded on the same continuous scale described in the Fig. 5 caption. See text for discussion.

Figure 8. Frequency histogram of projected *C. bezziana* wing image configuration scores on PCs 1-28 onto the CVA discriminant axis separating African and Asian (Sumba) populations. The between-groups separation is significant at the $\alpha < 0.01$ level as assessed by a bootstrap test of the log-likelihood ratio index.

Figure 9. *Chrysomya bezziana* wing image models constructed at the ends of the of the distributions of image projections onto the linear discriminant axis (CV-1) that separates African and Asian (Sumba) wing image data. Distinctions between these images represent the major morphological distinctions between the wings of these populations on a pixel-by-pixel basis. Numbers below the hypothetical image models represent the coordinate values at which the models were constructed. The final graphic is an image difference map in which the values of the differences between pixel brightness values have been colour-coded on a continuous scale as described in the Fig. 5 caption. See text for discussion.

Figure 10. Projection of the *C. bezziana*, *C. megacephala*, and *C. rufifacies*, Procrustes-aligned, wing image configuration data into the space formed by the first three principal

components of the image covariance matrix. This subspace represents c. 60% of the image variation recorded by the reduced resolution wing image dataset. Note the pronounced, but far from perfect, tendency toward species separation, relative distinctiveness of *C. bezziana*, and presence of wing configuration subgroups and outliers within both *C. bezziana* and *C. megacephala* within the PC-1 vs. PC-2 subspace.

Figure 11. Projection of the *C. bezziana*, *C. megacephala A*, and *C. rufifacies*, scores on PCs 1-32 into the space formed by the two CVA discriminant axes. These axes represent 100% of the difference between group centroids in the linear, eigenvalue-standardized ordination space. Note tightness of variation within each of the species clusters, the clear and clean separation of species clusters from one another and the orientation of between-species distinctions relative to those of the discriminant axis vectors.

Figure 12. Wing image models constructed at the ends of the of the distributions of image projections along the two species-difference linear discriminant axes (CV-1, CV-2). Distinctions between these images represent the major models of digital image distinction on a pixel-by-pixel basis. Numbers below the hypothetical image models represent the coordinate values at which the models were constructed. The final column contains pixel difference maps in which the values of the differences between pixel brightness values have been color coded on a continuous scale as described in the Fig. 5 caption. See text for discussion.

Figure 13. Projection of the *C. bezziana* major axis-aligned, wing image configuration data into the space formed by the first three principal components of the image covariance matrix for the gender-difference dataset. This subspace represents c. 48% of the image variation recorded by the reduced resolution image set. Note the strong, but not perfect, separation between male and female cohorts along PC-2, the presence of image configuration subgroups within the female dataset, and the difference in the image configuration variance between the two sexes.

Figure 14. Frequency histogram of the projections of *C. bezziana* scores on PCs 1-27 onto the CVA discriminant axis separating Asian (Sumba) male and female populations. The between-groups separation is significant at the $\alpha < 0.01$ level as assessed by a bootstrap test of the log-likelihood ratio index.

Figure 15. *Chrysomya bezziana* wing image models constructed at the ends of the distributions of image projections along the Asian (Sumba) male - female linear discriminant axis (CV-1). Distinctions between these images represent the major models of digital image distinction on a pixel-by-pixel basis. Numbers below the hypothetical image models represent the coordinate values at which the models were constructed. The final column contains a pixel difference maps in which the values of the differences between pixel brightness values have been colour-coded on a continuous scale as described in the Fig. 5 caption. See text for discussion.